Geoderma 347 (2019) 210–219

Contents lists available at ScienceDirect

Geoderma

journal homepage: www.elsevier.com/locate/geoderma

Mineralogical differences in a temperate cultivated soil arising from different agronomic processes and plant K-uptake

Eleanor Bakker[a], Bruno Lanson[a,*], Nathaniel Findling[a], Michelle M. Wander[b], Fabien Hubert[c]

[a] Univ. Grenoble Alpes, Univ. Savoie Mont Blanc, CNRS, IRD, IFSTTAR, ISTerre, F-38000 Grenoble, France
[b] Dept Natural Resources and Environmental Sciences, Univ. Illinois at Urbana-Champaign, Urbana, IL, USA
[c] Univ. Poitiers, CNRS, IC2MP, F-86000 Poitiers, France

ARTICLE INFO

Handling editor: David Laird

Keywords:
Potassium (K)
Plant nutrition
Fertilisation
Clay mineralogy
X-ray diffraction
Long-term field experiment
Morrow plots

ABSTRACT

Potassium (K) is an essential plant nutrient mainly present in the crystal structure of K-bearing soil minerals (K-feldspars, micas). To assess the evolution of (clay) mineralogy due to K^+ release from these minerals in continuously cultivated soils, samples were collected from long-term (1904–2014) field experiments submitted to contrasting crop rotations and amendments, with and without fertilisation. Soil samples were size-fractionated and mineralogy of the silt fraction and of clay subfractions was determined quantitatively by modelling X-ray diffraction (XRD) patterns. Clay subfractions were also analysed for their cation exchange capacity (CEC).

Mineralogical data indicate the stability of clay mineralogy and the increased abundance of the finest clay subfraction at the expense of coarser ones, regardless of agronomic practices or amount of K removed by plants. This increase is accompanied by an increase in the bulk clay CEC owing to the major contribution of the finest clay subfraction to this parameter. Mineral dissolution, rather than alteration of mineral phases from coarse clay subfractions, most likely supplements K for plant nutrition in this soil. Dissolution is favoured over cation exchange owing to the dioctahedral character of micas and to their fine-grained granulometry. The observed long-term mineralogical resilience also indicates that part of plant nutrition is obtained from subsoil in a non K-limited context, whereas K supply through K-feldspar dissolution appears marginal.

1. Introduction

Potassium (K) is an essential plant nutrient, playing roles in photosynthesis, water regulation and plant resistance to diseases (Marschner, 1995; Mengel et al., 2001). In soils, 98–99% of the potassium is found in the crystal structure of K-bearing minerals such as K-feldspars and micas (muscovite and biotite – Brouder, 2011; Mengel et al., 2001; Sparks, 1987). In addition to climate, vegetation and factors like soil texture and pH, content and composition of soil solution, the nature and extent of weathering of K-bearing minerals present control the release of mineral K into solution through dissolution (Manning et al., 2017; Mengel et al., 2001; Sparks, 1987; Velde and Barré, 2009). Apart from this mineral pool, K is found also as an exchangeable cation (1–2%) and in the soil solution (0.1–0.2% – Brouder, 2011; Mengel et al., 2001; Sparks, 1987). Recent evaluations of K-testing methods and their interpretation suggest however that common categories used to describe K in soils (soluble, exchangeable, fixed) are not universally agreed upon or understood and that renewed exploration of mineralogical controls over K cycling and interlayer K contributions to plant nutrition are needed (Brouder, 2011).

Whilst exchangeable K, weakly held by the surface charges of clay minerals, and solution K are readily available for uptake by plants, release of mineral K which is present in the interlayer space of high-charge 2:1 clay minerals (micas) is thought to require depletion of exchangeable and solution K to low concentration (Smith and Scott, 1966). Concentrations associated with such K release from high-charge 2:1 clay interlayers are known to vary with the initial mica crystal structure, ranging from 2.3 to 16.8 $\mu g\,mL^{-1}$ for trioctahedral micas to $< 0.1\ \mu g\,mL^{-1}$ for dioctahedral muscovite and illite (Rausell-Colom et al., 1965; Sparks, 1987). The former K concentrations are compatible with those reported in soil solutions (4–40 $\mu g\,mL^{-1}$, Hinsinger, 1998) whereas the latter ones were only reported in the close vicinity (~1 mm) of plant roots where mineral dissolution may be significant (Jungk and Claassen, 1997; Jungk et al., 1982). The possible release of mineral K^+ from mica interlayers and substitution by other cations is most often intimately related to clay mineralogical alteration, and more especially to the lowering of layer charge deficit (Hinsinger, 1998; Marschner, 1995; Mortland et al., 1956; Tributh et al., 1987; Walker,

* Corresponding author.
E-mail addresses: eleanorbakker@outlook.com (E. Bakker), bruno.lanson@univ-grenoble-alpes.fr (B. Lanson).

https://doi.org/10.1016/j.geoderma.2019.04.010
Received 8 January 2019; Received in revised form 4 April 2019; Accepted 6 April 2019

1950). Clay particle size may also influence the release of mineral K from clay minerals, which decreases with decreasing particle size (Doll et al., 1965; Reed and Scott, 1962; Scott and Reed, 1962b; Scott and Smith, 1966).

The ability of plants to recover K from clay minerals has been observed in laboratory experiments from the vermiculitisation of K-bearing micas induced by plants grown on clay substrates (Barré et al., 2007, 2008a; Hinsinger and Jaillard, 1993; Hinsinger et al., 1992; Niebes et al., 1993). The extent to which plants can extract K varies notably with plant species, proximity to plant roots, soil solution chemistry and clay mineralogy (Barber and Mackay, 1986; Boyle and Voigt, 1973; Kraffczyk et al., 1984; Marschner, 1995; Rengel and Damon, 2008; Schenk and Barber, 1980; Scott and Reed, 1962a). Long-term field experiments that began in the 19th and 20th centuries have led to the view that continuous cropping (30–135 years) increases smectite and/or vermiculite contents at the expense of mica/illite (Dissing Nielsen and Møberg, 1984; Møberg and Dissing Nielsen, 1983; Tributh et al., 1987). Surprisingly, Singh and Goulding (1997) observed an increase in the average K-concentration of soils from the Broadbalk continuous wheat plots established in 1843 at the Rothamsted Experimental Station (UK). The average total K-concentration increased from 1.01% (in 1856) to 1.10% and 1.20% in 1987 in non K-fertilised and K-fertilised plots, respectively, but no significant modification of clay mineralogy was detected.

In the aforementioned studies, clay mineralogy was determined using qualitative X-ray diffraction (XRD) methods that rely on the description of sharp and well-defined peaks associated with discrete clay minerals. Such qualitative description of XRD data does not recover comprehensive information about clay mineralogy and fails to measure contributions from mineral fractions potentially highly reactive: i) extremely small or crypto-crystalline and ii) complex interstratified minerals are essentially overlooked owing to their weakly modulated and faint diffraction signatures (Lanson, 2011). Over the last two decades, the peak decomposition method has improved and rationalised interpretation of XRD data, by decomposing profiles into elementary contributions that allow identifying contributions from both discrete and interstratified clay minerals (Lanson, 1997). Composition of the latter may be derived from the comparison with calculated patterns (e.g., Reynolds Jr, 1985). As a result, shifts in the position of diffraction maxima and/or composition of mixed layers have been correlated to changes in K-concentration and to K-fertilisation (Barré et al., 2008a, 2008b; Pernes-Debuyser et al., 2003; Velde and Peck, 2002). In their study of the Morrow Plots long-term experiment, Velde and Peck (2002) reported with this approach the apparent illite-depletion of the clay fraction from the continuous corn plot, whereas no evolution was detectable for the three year rotation (corn-oats-hay) plot. As calculated from yearly yields and fertiliser inputs, both plots exhibit similar K balance over the recent (1955–2005) period, however (Table 1 – Khan et al., 2014). On the other hand, these authors reported mineral stability in both the unfertilised crop rotation plot and the fertilised continuous corn plots despite negative and positive K balances, respectively (Table 1 – Khan et al., 2014). In any case, despite improving the description of clay mineral phases to include mixed layers and providing a proxy to their composition, the peak decomposition method does not account for the whole XRD profile and the obtained information remains essentially qualitative. In addition, the decomposition method does not allow taking into account highly-disordered and/or interstratified contributions with small particle size.

More recently, a full-profile modelling method has been developed and used to characterise clay mineralogy of hydrothermal and diagenetic sequences (Aplin et al., 2006; Drits et al., 1997; Inoue et al., 2005; Lindgreen et al., 2000; McCarty et al., 2004; Sakharov et al., 1999a, 1999b). This approach has been adapted for soil samples and allows investigating soil mineralogy in a quantitative manner (Hubert et al., 2009, 2012; Viennet et al., 2015). Quantitative mineralogy appears especially important in the perspective of expected increases in fertilisation and competition for arable land resources, but also for the growing interest in CO_2 sequestration in cultivated soils (DeFries et al., 2010; Lambin and Meyfroidt, 2011; Mueller et al., 2012). It is evident that comprehensive and quantitative descriptions of soil (clay) mineralogy are key to the assessment of soil responses to land-use changes or fertiliser inputs, given the contradictory results obtained from studies based on qualitative analyses of XRD data (see for example Dissing Nielsen and Møberg, 1984; Singh and Goulding, 1997; Tributh et al., 1987). The aim of the present study was thus to obtain a comprehensive compositional description of the clay minerals from the Morrow Plots by using full-profile XRD modelling and to compare and contrast, quantitatively, the effects of 110 years of continuous plant-growth under different agronomic treatments on the nature and potassium content of clay minerals in the soil.

Table 1
Impact of agronomical practices on K content and balance.

	CU	CF	RU	RF
Exchangeable K content in surface soil (0–15 cm) from 1955 (kg K ha^{-1})[a]	242		217	
Soil K content (1969–1995)[b] kg K ha^{-1}	250.7	317.2	241.7	266.5
Exchangeable K content in surface soil (0–15 cm) from 2005 (kg K ha^{-1})[a]	403	354	382	332
K balance (1955–2005)[c] kg K ha^{-1}	−892	+539	−1088	+249

[a] Exchangeable K contents determined in 1955 and 2005 samples (0–15 cm – Aref and Wander, 1998).

[b] K contents are average values from samples collected annually from 1969 to 1995 (0–15 cm – Aref and Wander, 1998).

[c] K balance values are computed from yearly yields and fertiliser inputs. See Khan et al. (2014) for details.

2. Materials and methods

2.1. Location and characteristics

The Morrow Plots (MP) are located on the Urbana-Champaign campus of the University of Illinois (USA). The soil is an Aquic Argiudoll (loessic Flanagan silt loam – USDA soil taxonomy) developed on glacial till under temperate grassland vegetation. The MP receive an average of 968 mm precipitation (576 mm snowfall) per year, with a yearly average temperature of 11.1 °C (1904–2014 – MRCC, 2018). The MP have been under continuous cultivation since their establishment in 1876 and are accompanied by an extensive record of crop species, rotations, fertiliser inputs and yields (Aref and Wander, 1998; Odell et al., 1984). Ten plots were established initially, and of these only three now remain. Each of the remaining plots is subject to a different crop rotation. Plot #3 is planted with corn (*Zea mays*) every year (C plots). Plot #4 (not included in this study) was initially planted in a two-yearly corn-oats (*Avena sativa*) rotation before being changed to a two-yearly corn-soybeans (*Glycine max*) rotation in 1967 to match regional cropping practices. Plot #5 is planted in corn-oats-hay on a three-yearly rotation (R plots), where the hay crop was red clover (*Trifolium pratense*) from 1904 to 1954 and alfalfa (*Medicago sativa*) from 1955 onwards. Corn hybrids have been introduced in the rotations since 1937. Each of the plots is now divided into eight subplots, which each have a different fertilisation history. In the present study, samples were obtained from subplots which have remained unfertilised (CU and RU subplots) from the start of the experiment in 1876, and from subplots unfertilised between 1876 and 1954 which have received a nitrogen-phosphate-potassium (NPK) fertilisation treatment since 1955 (CF and RF subplots). Fertiliser is applied every year in CF subplot and once every three years (when corn is planted) in RF subplot. Fertilisation allowed for positive K balances in both CF and RF subplots, whereas Khan et al. (2014) computed negative balances for the equivalent unfertilised subplots (CU and RU subplots – Table 1). Even for unfertilised

subplots, soil K tests exhibit rather high values for soils cropped continuously for over a century (Table 1 – Aref and Wander, 1998). The seeding density of F subplots was also increased in 1955. Only minor adjustments have taken place since 1955, most notably a change from mouldboard to chisel plough in 1989 and an increase in seeding density in 2013. In 2013 and 2014, sampling took place from the 0–25 cm surface horizon on fallow plots just after harvest (late-September to October). Unfertilised samples from 1904 Plots #3 and #5, and both fertilised and unfertilised subplots from 1957, 1980 and 1997 were collected from the soil archive at the U. of Illinois – Department of Agriculture (0–20 cm horizon). The latter samples were initially taken in the fall after harvest (Bob Dunker—Univ. of Illinois, personal communication). A complete description of the MP experimental fields can be found in Odell et al. (1984) and Aref and Wander (1998), where the samples in the current study are from NB (F) and NC (U) subplots of Plots #3 (C) and #5 (R).

2.2. Size-fractionation

Air dried samples were first sieved at 2000 µm to remove large organic fragments. Approximately 5 g, accurately weighed, of < 2000 µm soil material were dispersed via sonication in Milli-Q water (18.2 MΩ cm^{-1}) before being wet-sieved to 50 µm (10 g of starting material were used for 2013 and 2014 samples). The 2000–50 µm fraction obtained was dried at 50 °C. The < 50 µm fraction was centrifuged and flocculated with NaCl to reduce water content, then subjected to three overnight NaCl (2 M) saturation cycles, followed by centrifugation and washing in dialysis tubes (Spectre/Por 6–8 kD membrane) until chloride free. Milli-Q water was systematically used for solution preparation, washing and dispersion steps of sample fractionation and preparation. Sequential size fractionation was then performed by repeated centrifugation using a Beckmann-Coulter Avanti J-20XP centrifuge (procedure adapted from Hubert et al., 2012). A JS 4.3 swinging bucket rotor was used to separate 50–2 and < 2 µm fractions, with the 50–2 µm fraction set aside to dry in the oven at 50 °C. 10 repetitions were performed to obtain a clear supernatant, with dispersion via sonication (30 s) between successive cycles. 2–0.2, 0.2–0.05 and < 0.05 µm subfractions were obtained from repeated centrifugation of the initial < 2 µm fraction using a JS 24.38 swinging bucket rotor, with 10–15 cycles being necessary to obtain a clear supernatant for each subfraction. 1 M $CaCl_2$ or KCl was then used to saturate subfractions with either Ca^{2+} or K^+ (three 24 h cycles) and samples were dialysed until chloride-free.

2.3. Chemical analyses

Bulk < 2 µm fractions from 1904, 1957 and 2014 (CF and RU subplots – CU and RU for 1904) were analysed for major and trace elements by inductively coupled plasma optical emission after sample preparation according to Carignan et al. (2001). These samples were analysed also for C, H, and N to determine their organic composition. Cation exchange capacity (CEC) analysis was also performed on these bulk < 2 µm fractions, and on 2–0.2, 0.2–0.05, and < 0.05 µm subfractions of 2014 samples (CF and RU subplots) using the cobalt hexamine method (Dohrmann and Kaufhold, 2009; Orsini and Remy, 1976).

2.4. X-ray diffraction analysis

X-ray diffraction (XRD) analysis of < 2 µm subfractions was performed on Ca-saturated oriented slides prepared via the pipette method, under air-dried (Ca-AD) or ethylene glycol (Ca-EG) saturated conditions. The mass of sample present on each slide was determined and used for subsequent XRD profile modelling. EG solvation was ensured through vapour exposure at 50 °C overnight. Oriented slides of selected K-saturated samples were also analysed following heat treatments at 150 or 350 °C for 4 h (K-150 and K-350 samples, respectively). Samples were allowed to cool to room temperature before XRD data collection. XRD patterns of Ca-AD and Ca-EG samples were collected at 40% relative humidity using a Bruker D8 equipped with an Anton Paar CHC+ chamber coupled to an MHG Messtechnik humidity controller. Patterns of K-150 and K-350 samples were collected at 5% relative humidity with the same instrument. A Sol-XE Si (Li) solid state detector from Baltic Scientific Instruments was used to record intensities using CuKα radiation over 2–50°2Θ using 0.04° steps-and a counting time of 6 s per step for < 2 µm subfractions. 50–2 µm fractions were prepared for randomly oriented powder XRD analysis by milling with ethanol in a McCrone® micronising mill for 8 min. XRD data was collected over 3–90°2Θ with 0.026° steps and a 8 s counting time per step using the Bruker D8 diffractometer. In all cases, the sizes of the divergence slit, the two Soller slits and the antiscatter slit were 0.3°, 2.5°, 2.5° and 0.3°, respectively.

2.5. XRD full-profile modelling

Qualitative analysis of the < 2 µm subfractions was carried out as described in Bakker et al. (2018) where a detailed description of phase identification procedure is found. Full-profile XRD pattern modelling was then performed with the Sybilla programme developed by Chevron™ (Aplin et al., 2006). Parameterisation and fitting procedure described in Bakker et al. (2018) were used for all samples and subplots from 1904 to 2014. Briefly, this modelling is based on the direct comparison between experimental and calculated 00*l* XRD reflections, and fitting takes place via trial-and-error determination of structure factors to arrive at a single structure model which fits both the Ca-AD and Ca-EG XRD profiles of < 2 µm subfractions (Drits et al., 1997; Hubert et al., 2009, 2012; Sakharov et al., 1999a, 1999b; Viennet et al., 2015). Such an approach relies on differences in layer-to-layer distances and structure factors for expandable layers arising from the different treatments (Ca-AD and Ca-EG) and leads to the determination of the proportion or weighted concentration of each independent phase in the sample.

Both discrete and interstratified contributions were considered. In the latter, factors such as layer types, their proportions and stacking sequences were refined. A single structure model which fits both the Ca-AD and Ca-EG XRD profiles of < 2 µm subfractions is obtained at the end of the procedure. Discrete chlorite, kaolinite, illite and smectite were identified in < 2 µm subfractions, in addition to up to seven mixed-layer contributions. The Profex interface for BGMN software (Doebelin and Kleeberg, 2015) was used for quantitative phase analysis through the Rietveld refinement of XRD patterns from the 50–2 µm fractions.

3. Results

3.1. Granulometry

Results of size-fractionation are presented in Fig. 1. Recovery was 90.7–97.8% of the starting weight (94.9% on average). Individual results show a high and non-systematic scatter between subplots for a given year, and for a single subplot in different years (Fig. S1). As a result of this variability, plots were assessed on the basis of the cropping practices; yearly averages were also considered. When averaged over all subplots for a given year, the 2000–50 µm fraction represents 7% (± 2%), the 50–2 µm fraction 64% (± 2%), and the < 2 µm fraction 29% (± 2%), for the years 1957 to 2014 (Fig. 1a). No systematic variation was observed between subplots for these fractions as a result of cropping practices (Figs. 1b–d, S1). These values are 4, 62, and 33%, respectively, for 1904. The proportions of the 2–0.2, 0.2–0.05 and < 0.05 µm subfractions are also significantly different for 1904 compared to other years, most likely indicating sample grinding, consistent with the absence of soil aggregates in the sampled jar. When looking at the

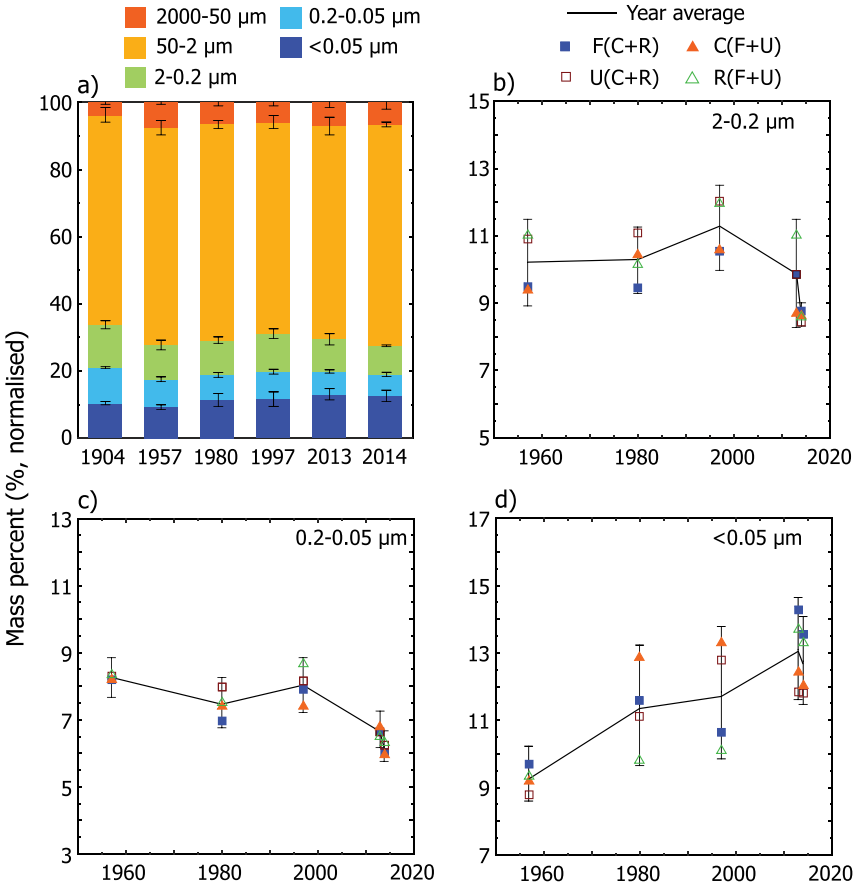

Fig. 1. Grain size distributions obtained for 1904–2014 soil samples with the sequential fractionation procedure described in the text; a) Size distribution of the < 2000 µm fraction averaged over all subplots for a given year and normalised to 100%, b–d) Abundances of clay subfractions for different agronomic practices. Solid black lines represent the yearly average for each subfraction (b: 2–0.2 µm, c: 0.2–0.05 µm, and d: < 0.05 µm subfraction); esd's on illite content are calculated from all subplots for a given year. (For interpretation of the references to colour in this figure, the reader is referred to the web version of this article.)

relative proportions of < 2 µm subfractions averaged over all subplots in a given year (Fig. 1d), there is a tendency for the < 0.05 µm subfraction to increase from ~9% of total sample mass in 1957 to ~13% in 2013–2014 (Fig. 1d). At the same time the relative mass of the 0.2–0.05 µm subfraction decreases by ~2% whereas that of the 2–0.2 µm subfractions is about stable (possible decrease by ~1 mass % – Fig. 1b–c). In addition, minor differences can be observed between the proportions of 2–0.2 µm subfractions of C and R subplots, C subplots containing generally slightly less mass than corresponding R subplots (Fig. 1b). The inverse is observed for < 0.05 µm subfractions, where C subplots tend to have a greater proportion of < 0.05 µm subfraction than corresponding R subplots, except for recent years. These differences are statistically insignificant over the period studied, however.

3.2. Chemical analyses

Elemental analyses (Table 2) are consistent with a soil clay fraction dominated by phyllosilicates, with high levels of SiO_2 (43–46%) and Al_2O_3 (17–19%). K levels were similar in both subplots in 1904 (2.13% K_2O), and did not vary between 1904 and 1957 (2.15%). These levels are similar to those reported for clay fractions from a variety of soils of similar origin (Doll et al., 1965; Singh and Goulding, 1997). Whilst K decreased in clay fractions from both RU and CF subplots since 1957, the rate of decrease in RU subplots (−16%) is faster than that in CF subplots (−7%). In 1904, the C/N ratio of the RU subplot (11.3) was greater than that of CF (9.5). For both subplots, the C/N ratio has decreased since 1904 in line with the systematic loss of carbon. The carbon decrease rate has slowed in CF subplots since 1957 and the introduction of fertilisation, whilst C levels continue to decrease at a similar rate post-1957 in RU subplots. The CEC of the < 2 µm fraction measured for 1904 is similar for CU and RU subplots and remains constant between 1904 and 1957 (Table 2). From 1957, the CEC of both C and R subplots increases significantly (by ~15%) from 48 to 55 $cmol_c\,kg^{-1}$ in 2014 for both CF and RU subplots. In addition, CEC of the < 0.05 µm subfractions are akin in these two subplots at 81–82 $cmol_c\,kg^{-1}$ (sample 2014) On the other hand, 0.2–0.05 and 2–0.2 µm subfractions demonstrate a difference of 7–8 $cmol_c\,kg^{-1}$ favouring RU subplots (Table 3).

Table 2
Results of CEC and elemental analyses for the bulk Na-saturated < 2 µm fraction from samples 1904, 1957 and 2014.

Year	Fraction	CEC	C	N	C/N	K_2O	Na_2O	MgO	CaO^1	TiO_2	Fe_2O_3	MnO	P_2O_5	SiO_2	Al_2O_3	LOI
		$cmol_c\,kg^{-1}$	%	%		%	%	%	%	%	%	%	%	%	%	%
1904 RU	< 2 µm	45.5	6.47	0.58	11.25	2.15	0.25	1.78	0.08	0.79	8.56	0.07	0.28	45.57	17.25	21.63
1904 CF	< 2 µm	47.8	6.29	0.66	9.53	2.11	0.21	1.82	0.07	0.91	8.71	0.13	0.26	44.64	17.40	22.34
1957 RU	< 2 µm	47.9	6.18	0.57	10.93	2.18	0.22	1.78	0.07	0.82	8.33	0.08	0.29	46.56	17.30	20.20
1957 CF	< 2 µm	47.9	6.18	0.49	9.09	2.13	0.17	1.97	0.06	0.84	9.12	0.13	0.24	45.96	18.75	22.38
2014 RU	< 2 µm	55.2	5.79	0.60	9.65	1.83	0.15	1.91	–	0.65	8.85	0.06	0.32	43.09	18.10	19.12
2014 CF	< 2 µm	55.3	4.24	0.49	8.73	1.98	0.17	2.01	–	0.75	9.20	0.06	0.43	45.38	19.06	22.70

Note: The low value of Ca is due to Na-saturation of samples prior to analysis.

Table 3
Measured and calculated CEC values for sample 2014 clay-size fractions and subfractions. The calculated CEC value for the bulk < 2 µm fraction is a weighted average of the CEC values measured for the different subfractions.

	2014 RU			2014 CF		
Subfraction	CEC (meas.) $cmol_c\ kg^{-1}$	Rel. prop. (wt%)	CEC (calc.) $cmol_c\ kg^{-1}$	CEC (meas.) $cmol_c\ kg^{-1}$	Rel. prop. (wt%)	CEC (calc.) $cmol_c\ kg^{-1}$
< 2 µm	55.2	–	57.8	55.3	–	52.9
2–0.2 µm	22.1	30.7	–	14.0	31.8	–
0.2–0.05 µm	58.6	25.6	–	51.3	23.0	–
< 0.05 µm	82.2	43.8	–	81.2	45.1	–

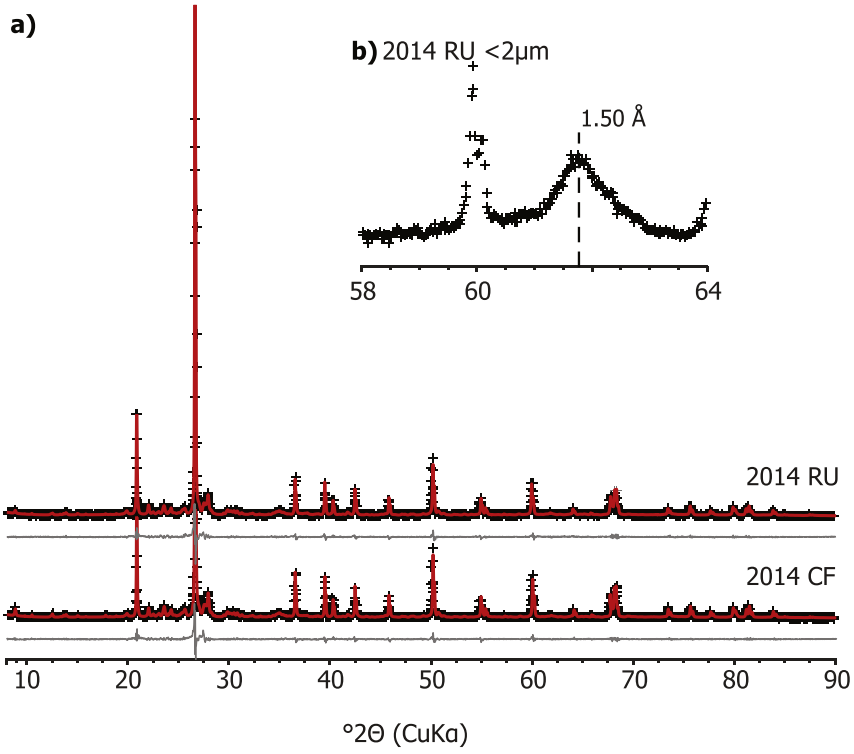

Fig. 2. Selection of quantitative phase analysis performed with the Rietveld method on XRD patterns of sample 2014 (CF and RU subplots). Experimental data is represented by black crosses, and solid red lines indicate the calculated intensity. Difference plots are solid grey lines underneath. Inset b) shows the position of the 06,33 reflection for the bulk < 2 µm fraction of sample 2014 (RU subplot). (For interpretation of the references to colour in this figure, the reader is referred to the web version of this article.)

3.3. XRD qualitative analysis and XRD profile simulation

Random powder XRD of 50–2 µm fractions and subsequent quantitative phase analysis found the mineralogy of the 50–2 µm fractions to be dominated by quartz (65–70%) and potassium- (10–13%) and plagioclase-feldspars (10–12% – Figs. 2 and S2a–d, Table S1). Mica, kaolinite and chlorite also contribute in minor amounts to this fraction (~5, 1 and 2% respectively), whereas trace amounts (< 1%) of calcite, anatase and amphibole were also identified. There is no systematic variation in mineralogy of 50–2 µm fractions from subplot-to-subplot or from year-to-year, with the exception of those of 1904 which had less mica and chlorite, presumably as the result of sample grinding (Table S1 and Fig. S2a–d). More especially, the relative abundances of K-bearing minerals (K-spars and micas) do not exhibit statistically significant evolutions with time and do not differ significantly as a function of agronomic practices (Table S1).

Full-profile modelling of the 2–0.2, 0.2–0.05 and < 0.05 µm subfractions for CF, CU, RF and RU subplots from 1904, 1957, 1980, 1997, 2013 and 2014 was performed using the structure model determined by Bakker et al. (2018) for the RU subplot. Similar contributions were used to model all < 2 µm subfractions from 1904 to 2014, with only limited modifications of their composition (layer-type proportions) and coherent scattering domain (CSD) sizes (Tables S2 and S3). The < 0.05 µm subfraction is dominated by randomly interstratified mixed layers in which illite, smectite and chlorite layers coexist (ISSCh). Two main contributions with contrasting illite contents (50 and 35% in ISSCh 50 and ISSCh 35, respectively) coexist in this finest subfraction with two additional ISSCh contributions, one dominated by illite (ISSCh 90), the other by smectite (ISSCh 5 – Tables S2c and S3c). Minor amounts of discrete smectite with extremely small CSD sizes and of kaolinite-illite (KI) complement the structure model of this < 0.05 µm subfraction. Except for discrete smectite, all contributions are present, with similar compositions and increased CSD sizes, in the 0.2–0.05 and 2–0.2 µm subfractions, together with discrete chlorite and discrete kaolinite. The peak at ~10 Å is accounted for by an additional illite-rich (ISSCh 80) mixed layer and discrete illite for the 0.2–0.05 µm and the 2–0.2 µm subfractions. Examples of the fit for 2014 CF and RU samples are shown in Fig. 3 whereas complete results of full-profile modelling of clay subfractions are reported in Tables S2 and S3. Experimental XRD patterns recorded for the same subfraction from different subplots or years show little variation in either peak position or intensity (Figs. S3a–d, S4a–d, and S5a–d). Consistently, very little mineralogical difference was noted in the results of the full-profile modelling. Similarly, the composition of the different mixed layers varies only slightly between different subfractions. For example, for 2014 CF subplot ISSCh 50 has a 52/26/22 layer composition in the < 0.05 µm subfraction which changes only slightly to 45/30/25 in the 2–0.2 µm subfraction (Ca-EG treatment - Table S3). This is fairly representative of the compositional evolution determined between fine and coarse clay subfractions for all subplots and phases. The content of smectite layers tends to decrease

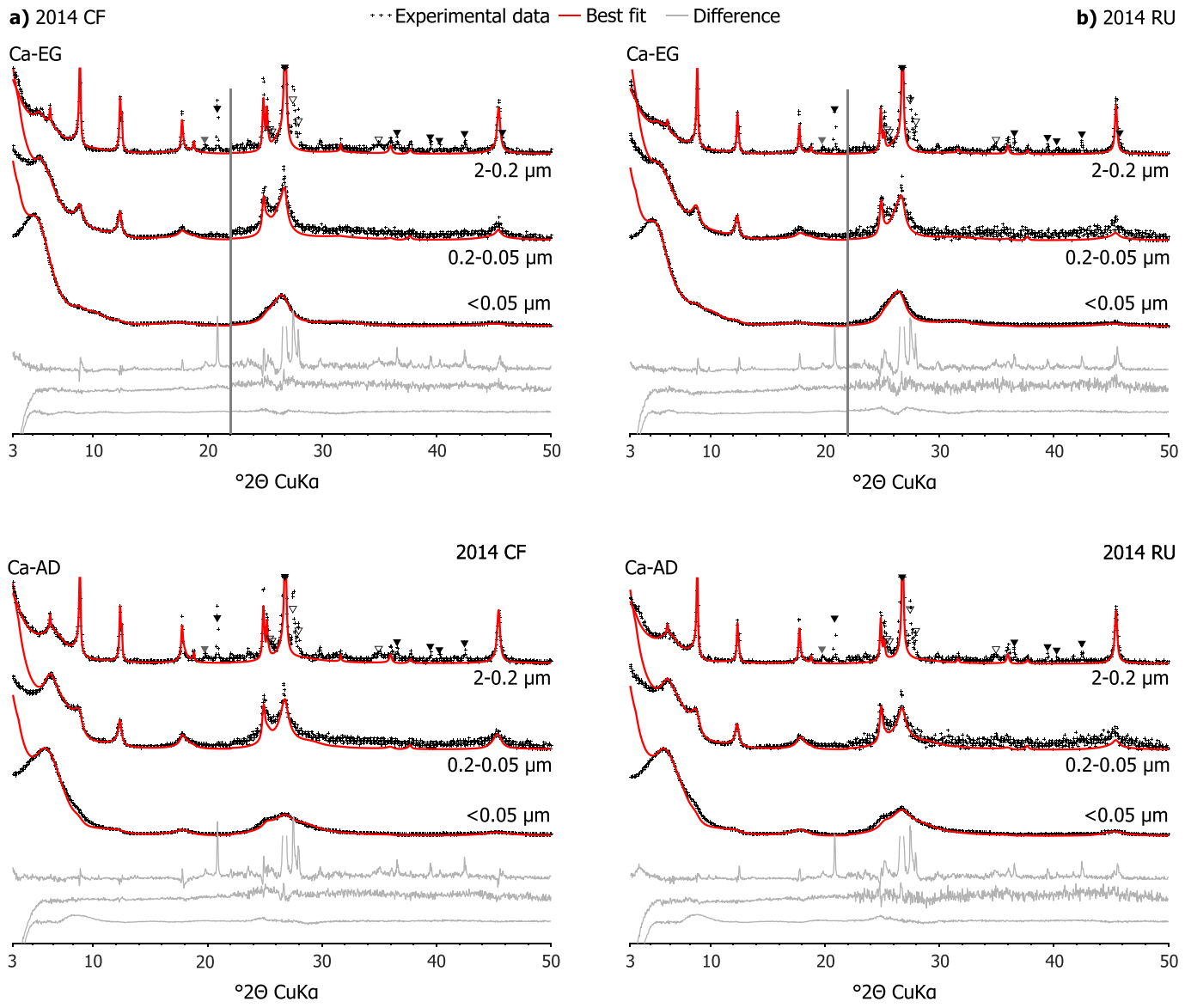

Fig. 3. Selection of XRD full-profile modelling of clay subfractions. a) 2014 RU (left) and b) 2014 CF (right) subplots. Ca-EG and Ca-AD are shown at the top and the bottom of the Figure, respectively. XRD patterns of 2–0.2, 0.2–0.05 and < 0.05 µm subfractions are shown from top to bottom for each treatment. Symbols as in Fig. 2. Quartz, feldspar, and *hk* contributions from phyllosilicates are indicated by solid black, open black and solid grey triangles respectively. These contributions were not taken into account during the modelling procedure. The vertical grey bars represents an increase in intensity of the high-angle region compared to the 2–22° 2θ angular range (×2 scale factor). (For interpretation of the references to colour in this figure, the reader is referred to the web version of this article.)

for 2–0.2 µm subfractions compared to finer subfractions whilst the proportion of illite layers decreases with increasing size subfraction for ISSCh 50, 35 and 5 but increases in ISSCh 90 and 80. These variations remain however marginal (~5% of all layers at most). Similarly, composition of individual contributions appears stable as a function of time. For example, the composition of ISSCh 50 in the < 0.05 µm subfractions varies from 55/23/22 (1904 CU), to 52/26/22 (1957 CF and 2014 CF), indicative of limited mineralogical evolution with time (Tables S2 and S3). Finally, K-spars are systematically present in the 2–0.2 µm clay subfraction, with no apparent evidence for an evolution of their relative contribution with time and/or agronomic practices (Fig. S3a–d).

Within each subfraction, proportions of the different layer types can be computed from the summation over all contributions of the proportion of this specific layer type within a contribution multiplied by the relative proportion of this contribution in the subfraction (Fig. 4). Proportions of illite, smectite and chlorite layers all increase in < 0.05 µm subfractions from 1957 to 2014, whilst the amount of kaolinite is stable (Fig. 4a). There is a concurrent decrease in the proportions of illite, smectite and chlorite layers with time in 0.2–0.05 µm subfractions, kaolinite content being again essentially stable (Fig. 4b). The proportion of illite layers in 2–0.2 µm subfractions shows considerable scatter, making it difficult to define a clear trend. The proportion of illite layers is however stable or marginally decreasing with time, whilst smectite layers also show a marginal decrease and chlorite and kaolinite layers are stable. All evolutions observed remain too marginal given the time period studied (60 years) to be statistically significant, the uncertainty on mixed layer composition being about ± 5% of a given layer type (Hubert et al., 2012; Lanson et al., 2009). These evolutions appear to be mostly linked to the evolution of gain size distribution within the < 2 µm fraction (Fig. 1). When all clay subfractions are considered jointly (Fig. 4d) the bulk clay mineralogy appears unchanged in the MP over the last 60 years of cropping, despite some intrinsic scatter.

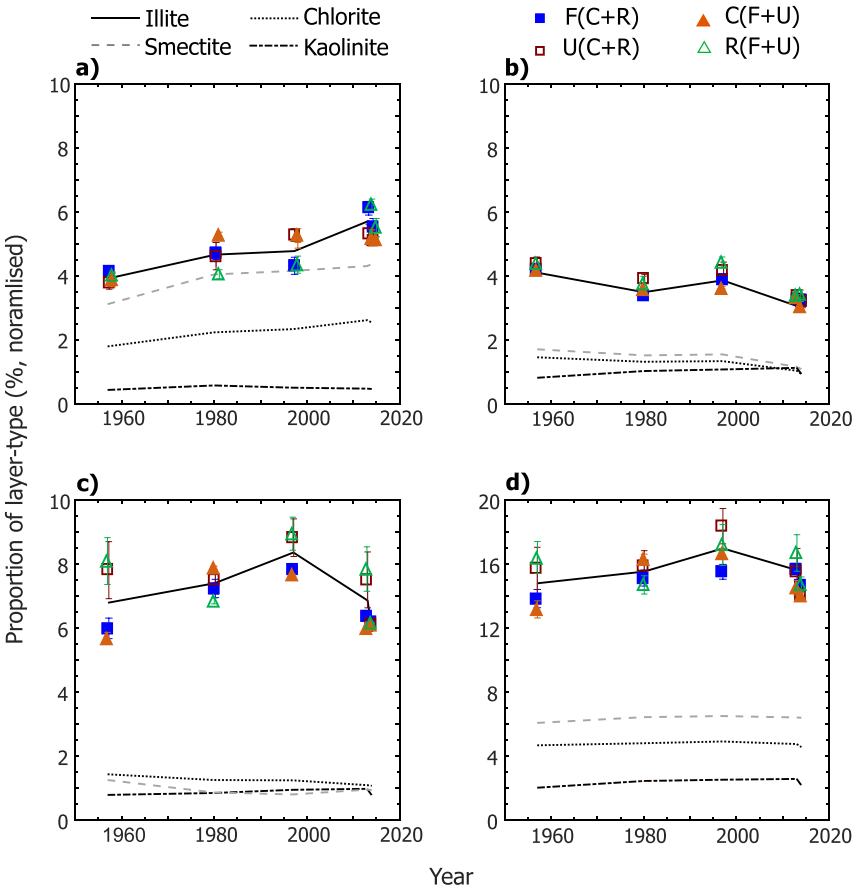

Fig. 4. Relative abundances of illite, smectite, chlorite and kaolinite layers in the different clay subfractions (a: < 0.05 µm, b: 0.2–0.05 µm, and c: 2–0.2 µm) and in the bulk < 2 µm fraction (d). Yearly averages are represented by lines, symbols representing different agronomic practices for illite. Smectite is represented in grey to enhance the difference between illite and smectite. Note the y-axis scale in d) is twice that of the other plots. Colour figure is available as Figure S6; esd's on illite content are calculated for C, R, U, and F subplots for a given year.

4. Discussion

4.1. Variability of results

The granulometry results show significant variability between subplots for a given year, this variation being non-systematic on a year-to-year-basis (Figs. 1a and S1). This variability is most likely related to heterogeneity within the MP, despite their small size, and is further indicative of the absence of systematic impact of crop rotation or fertilisation. Sampling date scatter is possibly an additional source of variability that must be taken into consideration, as the exact timing of sampling post-harvest is not well-defined for historic samples (fallow period after harvest). Planting dates in the plots have varied by as much as 147 days during the MP experiment, suggesting that harvest and therefore sampling dates are also subject to considerable variation (Aref and Wander, 1998). Given that numerous studies have related changes in soil properties over periods as short as two weeks (Collignon et al., 2012; Haines and Cleveland, 1981; Marschner, 1995; Mengel et al., 2001; Peoples et al., 2014; Turpault et al., 2008; Weaver and Forcella, 1979), sampling date scatter may play a role in the observed granulometric and mineralogical variability. Furthermore, analysis of yield and climate data of the MP from 1888 to 1996 (Aref and Wander, 1998) revealed that yield was positively correlated not only with the temperature and precipitation of the preceding November and December but also with those of the preceding year. Climatic fluctuations also affect the distribution of plant roots in soils, and therefore the location of nutrient uptake, and this variation may be significant on a year-to-year basis (Marschner, 1995; Mengel et al., 2001). The impacts of such climatic fluctuations on soil moisture and K availability may account, at least partially, for the difference observed between 2013 and 2014 samples despite their small separation in time. Fertilisation treatments represent another source of variability. Whilst NPK fertilisation positively influenced average yields in F subplots, yield stability dropped when rates of fertiliser application were increased (Aref and Wander, 1998), reflecting variations in the short term availability of plant nutrients.

4.2. Evolution of (clay) mineralogy

Following ~150 years of continuous cultivation, mineralogical differences in the MP are limited to a statistically insignificant increase of illite layers in 2–0.2 µm subfractions from U subplots compared to F subplots and of smectite layers in < 0.05 µm subfractions from C subplots compared to R ones (Fig. 4). In addition, K-spars are systematically present in the 2–0.2 µm subfraction, with no evidence of dissolution with time even in U subplots which exhibit strongly negative K-balances (Table 1; Fig. S3a–d), whereas the mineralogy of the coarser 50–2 µm is essentially independent of time and agronomic practices (Table S1 and Fig. S2a–d). Despite the presence of K-spars in clay subfractions, which is favourable to their dissolution (Manning et al., 2017; Sadusky et al., 1987), their contribution to K supply is thus likely limited. This long-term mineralogical stability is consistent with previous reports demonstrating that mineralogical differences reported between rhizosphere and bulk soil after 40 days of corn cultivation did not persist longer than a growth cycle (130 days – Adamo et al., 2016). This long-term resilience most likely indicates that soil K reserves exceed the plough layer and that a significant proportion of plant nutrition is obtained from subsoil in a non K-limited context (Hinsinger et al., 2017; Kautz et al., 2013; Khan et al., 2014; Kuhlmann, 1990; Marschner, 1995). The absence of K-limitation is substantiated by the observed yield increase in U subplots following the introduction of hybrid crops in 1937 (Aref and Wander, 1998), increase allowed by the high K-levels measured in non-amended soils cropped continuously for decades (217 and 242 kg K ha^{-1} measured in 1955 in R and C subplots,

respectively – Table 1). Furthermore, these soil K-test values systematically increase with time whatever the K-balance in the considered plot (Table 1). In addition to the likely subsoil contribution, the similarity between F and U subplots may be favoured by the higher seeding density in the former – 20,000 and 30,000 plants ha^{-1} in CU and RU subplots, respectively, versus 40,000 and 60,000 plants ha^{-1} (for 1957–1977 and 1978–2013, respectively) in F subplots (Odell et al., 1984).

The lack of mineralogical evolution with time reported by Bakker et al. (2018) for RU subplots is upheld in the present study that considers different subplots and treatments, thus indicating a minimal influence of agronomic practices on soil mineralogy. These results are in agreement with Velde and Peck (2002) for R subplots, but the latter authors reported a decrease in illite in the clay fraction of C subplots, based on XRD profile decomposition. The subtle variations in the position and shape of the 001 reflections in XRD profiles that were tentatively quantified by Velde and Peck (2002) were also observed in the present study. These were not systematic however and did not resolve into significant mineralogical differences following full-profile modelling, but rather contributed to the intrinsic sample variability.

Overall, the main evolution of clay mineralogy with time is the increased proportion of the < 0.05 µm subfraction from 1957 to 2014 for all subplots regardless of agronomic practices. This increase is accompanied by an increase of the bulk clay CEC owing to the major contribution of the finest subfraction to the CEC of the bulk < 2 µm fraction (Table 3). Contribution of soil organic matter to the CEC increase is likely minor despite decreasing C/N ratios with time. The minor character of this contribution is supported by similar CEC values measured for both CF and RU subplots despite the contrasting evolutions of their C/N ratios. The observed granulometric evolution of the bulk < 2 µm fraction is most likely due to mineral dissolution to supplement K for plant nutrition, as the K concentration decreases with time in this fraction for all subplots (Table 2). This decrease of K concentration is consistent with the negative K balances reported for U subplots over the period 1955–2005 (Khan et al., 2014). These authors calculated positive K balances for F subplots, however, whereas a decrease in total K is also observed, a seemingly contradictory result. The mineral contributions to all subfractions being essentially similar in composition (Tables S2 and S3), the observed evolution in grain size likely takes place through dissolution of the phases present in the coarser 2–0.2 and 0.2–0.05 µm subfractions rather than through their alteration or transformation. The breakdown of micro-aggregates initially present in these coarser subfractions could also account, at least partially, for the granulometric and CEC evolutions observed with time. This effect is likely minor, however, owing to the systematic presence of minor amounts of carbonates in all soil samples despite the slightly acidic soil pH (Table S1). Furthermore, the steady decrease in C concentration from 1904 to 2014 is essentially disconnected from the CEC increase, that occurs mainly from 1957 to 2014 (Table 2). Protection of < 0.05 µm particles by soil organic matter and sesquioxides, which are preferentially associated with this subfraction (e.g., Barré et al., 2014; Lützow et al., 2006; Singh et al., 2018), likely enhances the stability of this finest subfraction.

4.3. Mechanism of mineral K uptake by plants: Exchange vs. dissolution

As discussed above, both the absence of significant modification of clay mineralogy and the increased abundance of the finest clay subfraction (< 0.05 µm) at the expense of the coarser ones (0.2–0.05 and 2–0.2 µm subfractions) suggest that in the MP experiment K is most likely released from illite interlayer through dissolution rather than by exchange process. This inference raises the question of the prevalence of one process over the other and, more specifically, of the conditions leading to this predominance. Diffusion of K in illite interlayers at equilibrium in solutions similar to natural ones (de Haan et al., 1965; Nye, 1972) implies a negligible contribution of interlayer K exchange. However, early studies have unambiguously shown that K can be removed from K-rich mica interlayers (muscovite, illite, phlogopite, biotite) through the sole exchange process (Reed and Scott, 1962; Scott, 1986; Scott and Reed, 1962a, 1962b; Scott and Smith, 1966; Smith and Scott, 1966). In this case, the driving force is the chemical gradient between mica interlayers and the solution, and the limiting factor is thus the K concentration in solution; threshold concentrations in solution allowing K exchange range from 2.3 to 16.8 µg mL^{-1} for trioctahedral micas to < 0.1 µg mL^{-1} for dioctahedral muscovite and illite (Rausell-Colom et al., 1965; Sparks, 1987). The higher content of structural Fe(II) in natural trioctahedral micas, compared to dioctahedral ones, may be responsible for these contrasting behaviours, as Fe(II) oxidation decreases layer charge deficit, thus favouring the exchange of interlayer K^+ cations. Although low, these values allow for K exchange from trioctahedral micas in the laboratory (Hinsinger and Jaillard, 1993; Hinsinger et al., 1992; Niebes et al., 1993; Norouzi and Khademi, 2010), and in the field (Kapoor, 1972b; Wilson, 1966). The lower threshold concentrations determined for dioctahedral micas most likely hamper K exchange, however, consistent with the conclusions of Kapoor (1972a, 1972b), although root activity may induce such low concentrations in the rhizosphere (Hinsinger et al., 2011, 2017; Jungk and Claassen, 1997; Walker and Barber, 1962). The concentrations of other nutrients (e.g., P and NH_4^+) in solution may also have a key influence on the exchange of interlayer K, which can be totally inhibited in the presence of ~5 µmol L^{-1} of NH_4^+, a concentration common in natural soils (Springob, 1999).

Depending on the aforementioned experimental conditions, the kinetic competition between dissolution and exchange processes accounts for the heterogeneity of the results obtained from laboratory and field studies. Hinsinger and coworkers (Hinsinger et al., 1992, 1993; Hinsinger and Jaillard, 1993) showed unambiguously the prevalence of exchange leading to the fast vermiculitisation of coarse trioctahedral mica (2–100 µm phlogopite) by ryegrass and rape, possibly as the result of structural Fe(II) partial oxidation. Similar results were obtained by Naderizadeh et al. (2010) and Norouzi and Khademi (2010) also for trioctahedral micas (phlogopite and biotite) under alfalfa growth, whereas Vetterlein et al. (2013) reported a minor evolution of a reference illite (IMt-2, Clay Minerals Society Repository – < 20 µm particles) to illlite-expandable interstratification following 100 days of alfalfa growth. Conversely, no mineralogical evolution was reported for a natural soil (Vetterlein et al., 2013) or muscovite (Naderizadeh et al., 2010; Norouzi and Khademi, 2010), under similar experimental conditions. Muscovite dissolution even appears to be limited as alfalfa displays K deficiency symptoms (Norouzi and Khademi, 2010). Prevalence of dissolution was observed by Feigenbaum and Shainberg (1975) using Ca and H-resins to release K from illite interlayers.

Kinetic competition between dissolution and exchange processes was investigated directly by Viennet et al. (2016) in the specific context of K-vermiculite aluminisation under acidic conditions (trioctahedral high-charge clay mineral, pH = 3). These authors concluded that despite the faster release of both exchangeable (at the particle surface) and non-exchangeable interlayer (i.e. mineral) K for the finest size fraction investigated (0.1–0.2 µm), the exchange process was rapidly stopped. Release of interlayer K subsequently proceeds through stoichiometric dissolution of this finest size fraction, whereas exchange remains active for coarser fractions (1–2 µm and even more so for 10–20 µm). The decrease of K exchange when decreasing size fraction to clay size is consistent with experiments involving K release by chemical exchange (Doll et al., 1965; Reed and Scott, 1962; Scott and Reed, 1962b; Scott and Smith, 1966) or by cropping (Doll et al., 1965), whereas the increased dissolution rate of finer subfractions is supported by experimental studies (Acker and Bricker, 1992; Bray et al., 2015). Results of the present study support a marginal release of interlayer K by exchange mechanisms and the prevalence of dissolution over exchange, consistent with this general discussion, as MP surface soils are typified by fine-grained dioctahedral micas and clay minerals (inset

Fig. 2), both features being unfavourable to K exchange from mica interlayers.

5. Conclusions

Mineralogy of the silt fraction and of clay subfractions was determined quantitatively by modelling X-ray diffraction (XRD) patterns for a temporal series of top soil samples collected from the Morrow Plots long-term experimental fields. Samples from different subplots encompass a variety of cropping practices resulting in positive or negative K balances (fertilised and unfertilised subplots, respectively). Mineralogy of the different size fractions is essentially stable over time, independent of the overall K-balance and of agronomic practices, showing no significant decrease of the mica or K-spar relative abundances as the result of K uptake by plants. Within the clay fraction, the relative proportion of the finest (< 0.05 µm) subfraction increases with time, together with the cation exchange capacity of the bulk < 2 µm fraction. This systematic granulometric evolution results from the dissolution of illite-rich coarse clay fractions. Prevalence of dissolution over K-exchange to supply plants with needed K most likely results from the dioctahedral character of fine-grained micas present in the Morrow Plots. Subsoil provides additional K for plant nutrition, whereas contribution of K-feldspars appears minimal in a non K-limited context. Finally, the improved description of (clay) mineralogy allowed by the full-profile modelling approach did not allow to evidence significant variation of (clay) mineralogy possibly resulting from cropping practices and related K-uptake.

Acknowledgments

Martine Lanson (ISTerre, Grenoble, France) has coordinated all chemical analyses and has performed CEC measurements. Chemical analyses were performed at the Service d'Analyse des Roches et des Minéraux (SARM-CNRS, Vandoeuvre-lès-Nancy, France) for major elements and at the Institut de Chimie des Substances Naturelles (ICSN – Gif sur Yvette, France) for C, H and N. Paolo Benavides (ISTerre, Grenoble, France) is thanked for size fractionation and XRD analysis of 1980 and 1997 samples. Tauhid B. Khan (ISTerre, Grenoble, France) is thanked for preliminary investigations of MP samples. Financial support from INSU/EC2CO program to FH and BL is acknowledged (Project Claie, 2015-2016). ISTerre is part of Labex OSUG@2020 (ANR10 LABX56).

Appendix A. Supplementary data

Supplementary data to this article can be found online at https://doi.org/10.1016/j.geoderma.2019.04.010.

References

Acker, J.G., Bricker, O.P., 1992. The influence of pH on biotite dissolution and alteration kinetics at low temperature. Geochim. Cosmochim. Acta 56, 3073–3092.
Adamo, P., Barré, P., Cozzolino, V., Di Meo, V., Velde, B., 2016. Short term clay mineral release and re-capture of potassium in a *Zea mays* field experiment. Geoderma 264, 54–60.
Aplin, A.C., Matenaar, I.F., McCarty, D.K., van Der Pluijm, B.A., 2006. Influence of mechanical compaction and clay mineral diagenesis on the microfabric and pore-scale properties of deep-water Gulf of Mexico Mudstones. Clays & Clay Miner 54, 500–514.
Aref, S., Wander, M.M., 1998. Long-term trends of corn yield and soil organic matter in different crop sequences and soil fertility treatments on the Morrow Plots. Adv. Agron. 62, 153–198.
Bakker, E., Hubert, F., Wander, M.M., Lanson, B., 2018. Soil development under continuous agriculture at the Morrow Plots experimental fields from X-ray diffraction profile modelling. Soil Syst 2, 46.
Barber, S.A., Mackay, A.D., 1986. Root growth and phosphorus and potassium uptake by two corn genotypes in the field. Fert. Res. 10, 217–230.
Barré, P., Velde, B., Catel, N., Abbadie, L., 2007. Soil-plant potassium transfer: impact of plant activity on clay minerals as seen from X-ray diffraction. Plant Soil 292, 137–146.
Barré, P., Montagnier, C., Chenu, C., Abbadie, L., Velde, B., 2008a. Clay minerals as a soil potassium reservoir: observation and quantification through X-ray diffraction. Plant Soil 302, 213–220.
Barré, P., Velde, B., Fontaine, C., Catel, N., Abbadie, L., 2008b. Which 2:1 clay minerals are involved in the soil potassium reservoir? Insights from potassium addition or removal experiments on three temperate grassland soil clay assemblages. Geoderma 146, 216–223.
Barré, P., Fernandez-Ugalde, O., Virto, I., Velde, B., Chenu, C., 2014. Impact of phyllosilicate mineralogy on organic carbon stabilization in soils: incomplete knowledge and exciting prospects. Geoderma 235–236, 382–395.
Boyle, J.R., Voigt, G.K., 1973. Biological weathering of silicate minerals. Plant Soil 38, 191–201.
Bray, A.W., Oelkers, E.H., Bonneville, S., Wolff-Boenisch, D., Potts, N.J., Fones, G., Benning, L.G., 2015. The effect of pH, grain size, and organic ligands on biotite weathering rates. Geochim. Cosmochim. Acta 164, 127–145.
Brouder, S., 2011. Potassium cycling. In: Hatfield, J.L., Sauer, T.J. (Eds.), Soil Management: Building a Stable Base for Agriculture. Soil Science Society of America, Madison, WI, pp. 79–102.
Carignan, J., Hild, P., Mevelle, G., Morel, J., Yeghicheyan, D., 2001. Routine analyses of trace elements in geological samples using flow injection and low pressure on-line liquid chromatography coupled to ICP-MS: a study of geochemical reference materials BR, DR-N, UB-N, AN-G and GH. Geostand. Newslett. 25, 187–198.
Collignon, C., Ranger, J., Turpault, M.P., 2012. Seasonal dynamics of Al- and Fe-bearing secondary minerals in an acid forest soil: influence of Norway spruce roots (*Picea abies* (L.) Karst.). Eur. J. Soil Sci. 63, 592–602.
DeFries, R.S., Rudel, T., Uriarte, M., Hansen, M., 2010. Deforestation driven by urban population growth and agricultural trade in the twenty-first century. Nat. Geosci. 3, 178.
Dissing Nielsen, J., Møberg, J.P., 1984. The influence of K-depletion on mineralogical changes in pedons from two field experiments and in soils from four pot experiments. Acta Agric. Scand. (3), 391–399.
Doebelin, N., Kleeberg, R., 2015. Profex: a graphical user interface for the Rietveld refinement program BGMN. J. Appl. Crystallogr. 48, 1573–1580.
Dohrmann, R., Kaufhold, S., 2009. Three new, quick CEC methods for determining the amounts of exchangeable calcium cations in calcareous clays. Clays & Clay Miner 57, 338–352.
Doll, E.C., Mortland, M.M., Lawton, K., Ellis, B.G., 1965. Release of potassium from soil fractions during cropping. Soil Sci. Soc. Am. J. 29, 699–702.
Drits, V.A., Sakharov, B.A., Lindgreen, H., Salyn, A., 1997. Sequential structure transformation of illite-smectite-vermiculite during diagenesis of Upper Jurassic shales from the North Sea and Denmark. Clay Miner. 32, 351–371.
Feigenbaum, S., Shainberg, I., 1975. Dissolution of illite—a possible mechanism of potassium release. Soil Sci. Soc. Am. J. 39, 985–990.
de Haan, F.A.M., Bolt, G.H., Pieters, B.G.M., 1965. Diffusion of Potassium-40 into an illite during prolonged shaking. Soil Sci. Soc. Am. J. 29, 528–530.
Haines, S.G., Cleveland, G., 1981. Seasonal variation in properties of five forest soils in Southwest Georgia. Soil Sci. Soc. Am. J. 45, 139–143.
Hinsinger, P., 1998. How do plant roots acquire mineral nutrients? Chemical processes involved in the rhizosphere. Adv. Agron. 64, 225–265.
Hinsinger, P., Jaillard, B., 1993. Root-induced release of interlayer potassium and vermiculitization of phlogopite as related to potassium-depletion in the rhizosphere of ryegrass. J. Soil Sci. 44, 525–534.
Hinsinger, P., Jaillard, B., Dufey, J.E., 1992. Rapid weathering of a trioctahedral mica by the roots of ryegrass. Soil Sci. Soc. Am. J. 56, 977–982.
Hinsinger, P., Elsass, F., Jaillard, B., Robert, M., 1993. Root-induced irreversible transformation of a trioctahedral mica in the rhizosphere of rape. J. Soil Sci. 44, 535–545.
Hinsinger, P., Brauman, A., Devau, N., Gérard, F., Jourdan, C., Laclau, J.-P., Le Cadre, E., Jaillard, B., Plassard, C., 2011. Acquisition of phosphorus and other poorly mobile nutrients by roots. Where do plant nutrition models fail? Plant Soil 348, 29.
Hinsinger, P., Bell, M., White, P.J., 2017. Root traits and rhizosphere characteristics determining potassium acquisition from soils. In: Murrell, T.S., Mikkelsen, R.L. (Eds.), Frontiers of Potassium Science Conference. International Plant Nutrition Institute, Rome, Italy, pp. O289–O299.
Hubert, F., Caner, L., Meunier, A., Lanson, B., 2009. Advances in characterization of soil clay mineralogy using X-ray diffraction: from decomposition to profile fitting. Eur. J. Soil Sci. 60, 1093–1105.
Hubert, F., Caner, L., Ferrage, E., Meunier, A., 2012. Unraveling complex < 2 µm clay mineralogy from soils using X-ray diffraction profile modeling on particle-size subfractions: implications for soil pedogenesis and reactivity. Am. Mineral. 97, 384–398.
Inoue, A., Lanson, B., Marques Fernandes, M., Sakharov, B.A., Murakami, T., Meunier, A., Beaufort, D., 2005. Illite-smectite mixed-layer minerals in the hydrothermal alteration of volcanic rocks: I. one-dimensional XRD structure analysis and characterization of component layers. Clays & Clay Miner. 53, 423–439.
Jungk, A., Claassen, N., 1997. Ion diffusion in the soil–root system. In: Sparks, D.L. (Ed.), Adv. Agron. Academic Press, pp. 53–110.
Jungk, A., Claassen, N., Kuchenbuch, R., 1982. Potassium depletion of the soil-root interface in relation to soil parameters and root properties. In: Scaife, A. (Ed.), 9th Internation Plant Nutrition Colloquim. Commonwealth Agricultural Bureaux, Warwick, pp. 250–255.
Kapoor, B.S., 1972a. Weathering of micaceous minerals. Nor. Geol. Tidsskr. 52, 451–452.
Kapoor, B.S., 1972b. Weathering of micaceous minerals in some Norwegian podzols. Clay Miner. 9, 383–394.
Kautz, T., Amelung, W., Ewert, F., Gaiser, T., Horn, R., Jahn, R., Javaux, M., Kemna, A., Kuzyakov, Y., Munch, J.-C., Pätzold, S., Peth, S., Scherer, H.W., Schloter, M., Schneider, H., Vanderborght, J., Vetterlein, D., Walter, A., Wiesenberg, G.L.B., Köpke, U., 2013. Nutrient acquisition from arable subsoils in temperate climates: a review. Soil Biol. Biochem. 57, 1003–1022.

Khan, S.A., Mulvaney, R.L., Ellsworth, T.R., 2014. The potassium paradox: implications for soil fertility, crop production and human health. Renew Agric Food Syst 29, 3–27.
Kraffczyk, I., Trolldenier, G., Beringer, H., 1984. Soluble root exudates of maize: influence of potassium supply and rhizosphere microorganisms. Soil Biol. Biochem. 16, 315–322.
Kuhlmann, H., 1990. Importance of the subsoil for the K nutrition of crops. Plant Soil 127, 129–136.
Lambin, E.F., Meyfroidt, P., 2011. Global land use change, economic globalization, and the looming land scarcity. Proc. Nat. Acad. Sci. 108, 3465–3472.
Lanson, B., 1997. Decomposition of experimental X-ray diffraction patterns (profile fitting): a convenient way to study clay minerals. Clays & Clay Miner 45, 132–146.
Lanson, B., 2011. Modelling of X-ray diffraction profiles: Investigation of defective lamellar structure crystal chemistry. In: Brigatti, M.F., Mottana, A. (Eds.), Layered Mineral Structures and Their Application in Advanced Technologies. European Mineralogical Union Notes in Mineralogy Mineralogical Society Great Britain & Ireland, London, pp. 151–202.
Lanson, B., Sakharov, B.A., Claret, F., Drits, V.A., 2009. Diagenetic smectite-to-illite transition in clay-rich sediments: a reappraisal of X-ray diffraction results using the multi-specimen method. Am. J. Sci. 309, 476–516.
Lindgreen, H., Drits, V.A., Sakharov, B.A., Salyn, A.L., Wrang, P., Dainyak, L.G., 2000. Illite-smectite structural changes during metamorphism in black Cambrian Alum shales from the Baltic area. Am. Mineral. 85, 1223–1238.
Lützow, M.v., Kögel-Knabner, I., Ekschmitt, K., Matzner, E., Guggenberger, G., Marschner, B., Flessa, H., 2006. Stabilization of organic matter in temperate soils: mechanisms and their relevance under different soil conditions – a review. Eur. J. Soil Sci. 57, 426–445.
Manning, D.A.C., Baptista, J., Sanchez Limon, M., Brandt, K., 2017. Testing the ability of plants to access potassium from framework silicate minerals. Sci. Total Envir. 574, 476–481.
Marschner, H., 1995. Mineral Nutrition of Higher Plants, 2nd edition ed. Academic Press, London.
McCarty, D.K., Drits, V.A., Sakharov, B., Zviagina, B.B., Ruffell, A., Wach, G., 2004. Heterogeneous mixed-layer clays from the Cretaceous greensand, Isle of Wight, southern England. Clays & Clay Miner 52, 552–575.
Mengel, K., Kirkby, E.A., Kosegarten, H., Appel, T., 2001. Principles of Plant Nutrition. Springer, Dordrecht 849 pp.
Møberg, J.P., Dissing Nielsen, J., 1983. Mineralogical changes in soils used for potassium-depletion experiments for some years in pots and in the field. Acta Agric. Scand. 33, 21–27.
Mortland, M.M., Lawton, K., Uehara, G., 1956. Alteration of biotite to vermiculite by plant growth. Soil Sci. 82, 477–482.
MRCC, 2018. Cli-MATE: Midwestern Regional Climate Centre Application Tools Environment.
Mueller, N.D., Gerber, J.S., Johnston, M., Ray, D.K., Ramankutty, N., Foley, J.A., 2012. Closing yield gaps through nutrient and water management. Nature 490, 254.
Naderizadeh, Z., Khademi, H., Arocena, J.M., 2010. Organic matter induced mineralogical changes in clay-sized phlogopite and muscovite in alfalfa rhizosphere. Geoderma 159, 296–303.
Niebes, J.-F., Dufey, J., Jaillard, B., Hinsinger, P., 1993. Release of nonexchangeable potassium from different size fractions of two highly K-fertilized soils in the rhizosphere of rape (Brassica napus cv Drakkar). Plant Soil 155-156, 403–406.
Norouzi, S., Khademi, H., 2010. Ability of alfalfa (*Medicago sativa* L.) to take up potassium from different micaceous minerals and consequent vermiculitization. Plant Soil 328, 83–93.
Nye, P.H., 1972. The measurement and mechanism of ion diffusion in soils. VIII — a theory for the propagation of changes of pH in soils. J. Soil Sci. 23, 82–92.
Odell, R.T., Melsted, S.W., Walker, W.M., 1984. Changes in organic carbon and nitrogen of Morrow plots soils under different treatments, 1904–1973. Soil Sci. 137, 160–171.
Orsini, L., Remy, J., 1976. Utilisation du chlorure de cobaltihexamine pour la détermination simultanée de la capacité d'échange et des bases échangeables des sols. Bull. AFES - Sci Sol 4, 269–275.
Peoples, M.B., Richardson, A.E., Simpson, R.J., Fillery, I.R.P., 2014. Soil: Nutrient Cycling. In: Van Alfen, N.K. (Ed.), Encyclopedia of Agriculture and Food Systems. Academic Press, Oxford, pp. 197–210.
Pernes-Debuyser, A., Pernes, M., Velde, B., Tessier, D., 2003. Soil mineralogy evolution in the INRA 42 plots experiment (Versailles, France). Clays & Clay Miner 51, 577–584.
Rausell-Colom, J.A., Sweatman, T.R., Wells, C.B., Norrish, K., 1965. Studies in the artificial weathering of mica. In: Hallsworth, E.G., Crawford, D.V. (Eds.), Experimental Pedology. Univ. Nottingham 11th Easter School Agricutlural Science. Butterworths, London, pp. 40–72.
Reed, M.G., Scott, A.D., 1962. Kinetics of potassium release from biotite and muscovite in sodium tetraphenylboron solutions. Soil Sci. Soc. Am. J. 26, 437–440.
Rengel, Z., Damon, P.M., 2008. Crops and genotypes differ in efficiency of potassium uptake and use. Physiol. Plantarum 133, 624–636.
Reynolds Jr., R.C., 1985. NEWMOD: A Computer Program for the Calculation of One-dimensionnal Patterns of Mixed-layered Clays. Reynolds, R.C., Jr, Hanover, NH.
Sadusky, M.C., Sparks, D.L., Noll, M.R., Hendricks, G.J., 1987. Kinetics and mechanisms of potassium release from Sandy middle Atlantic coastal plain soils1. Soil Sci. Soc. Am. J. 51, 1460–1465.
Sakharov, B.A., Lindgreen, H., Salyn, A., Drits, V.A., 1999a. Determination of illite-smectite structures using multispecimen X-ray diffraction profile fitting. Clays & Clay Miner 47, 555–566.
Sakharov, B.A., Lindgreen, H., Salyn, A.L., Drits, V.A., 1999b. Mixed-layer kaolinite-illite-vermiculite in North Sea shales. Clay Miner. 34, 333–344.
Schenk, M.K., Barber, S.A., 1980. Potassium and phosphorus uptake by corn genotypes grown in the field as influenced by root characteristics. Plant Soil 54, 65–76.
Scott, A.D., 1986. Mechanisms of potassium release by soil minerals. In: XIII. Congress of International Society of Soil Science, Hamburg, Germany, pp. 1144–1154.
Scott, A.D., Reed, M.G., 1962a. Chemical extraction of potassium from soils and micaceous minerals with solutions containing sodium tetraphenylboron: II. Biotite. Soil Sci. Soc. Am. J. 26, 41–45.
Scott, A.D., Reed, M.G., 1962b. Chemical extraction of potassium from soils and micaceous minerals with solutions containing sodium tetraphenylboron: III. Illite. Soil Sci. Soc. Am. J. 26, 45–48.
Scott, A.D., Smith, S.J., 1966. Susceptibility of interlayer potassium in micas to exchange with sodium. Clays & Clay Miner. 14, 69–81.
Singh, B., Goulding, K.W.T., 1997. Changes with time in the potassium content and phyllosilicates in the soil of the Broadbalk continuous wheat experiment at Rothamsted. Eur. J. Soil Sci. 48, 651–659.
Singh, M., Sarkar, B., Sarkar, S., Churchman, J., Bolan, N., Mandal, S., Menon, M., Purakayastha, T.J., Beerling, D.J., 2018. Stabilization of soil organic carbon as influenced by clay mineralogy. In: Sparks, D.L. (Ed.), Adv. Agron. Academic Press, pp. 33–84.
Smith, S.J., Scott, A.D., 1966. Extractable potassium in grundite illite: I. method of extraction. Soil Sci. 102, 115–122.
Sparks, D.L., 1987. Potassium dynamics in soils. In: Stewart, B.A. (Ed.), Advances in soil science. Springer Verlag, New York, pp. 1–63.
Springob, G., 1999. Blocking the release of potassium from clay interlayers by small concentrations of NH4+ and Cs+. Eur. J. Soil Sci. 50, 665–674.
Tributh, H., Boguslawski, E.V., Lieres, A.V., Steffens, D., Mengel, K., 1987. Effect of potassium removal by crops on transformation of illitic clay minerals. Soil Sci. 143, 404–409.
Turpault, M.P., Righi, D., Uterano, C., 2008. Clay minerals: precise markers of the spatial and temporal variability of the biogeochemical soil environment. Geoderma 147, 108–115.
Velde, B., Barré, P., 2009. Soils, Plants and Clay Minerals. Springer, Berlin, Heidelberg.
Velde, B., Peck, T., 2002. Clay mineral changes in the Morrow experimental plots, University of Illinois. Clays & Clay Miner 50, 364–370.
Vetterlein, D., Kühn, T., Kaiser, K., Jahn, R., 2013. Illite transformation and potassium release upon changes in composition of the rhizophere soil solution. Plant Soil 371, 267–279.
Viennet, J.-C., Hubert, F., Ferrage, E., Tertre, E., Legout, A., Turpault, M.-P., 2015. Investigation of clay mineralogy in a temperate acidic soil of a forest using X-ray diffraction profile modeling: beyond the HIS and HIV description. Geoderma 241-242, 75–86.
Viennet, J.-C., Hubert, F., Tertre, E., Ferrage, E., Robin, V., Dzene, L., Cochet, C., Turpault, M.-P., 2016. Effect of particle size on the experimental dissolution and auto-aluminization processes of K-vermiculite. Geochim. Cosmochim. Acta 180, 164–176.
Walker, G.F., 1950. Trioctahedral minerals in the soil-clays of North-East Scotland. Mineral. Mag. 29, 72–84.
Walker, J.M., Barber, S.A., 1962. Absorption of potassium and rubidium from the soil by corn roots. Plant Soil 17, 243–259.
Weaver, T., Forcella, F., 1979. Seasonal variation in soil nutrients under six Rocky Mountain vegetation types. Soil Sci. Soc. Am. J. 43, 589–593.
Wilson, M.J., 1966. The weathering of biotite in some Aberdeenshire soils. Mineral. Mag. 36, 1080–1093.

Mineralogical differences in a temperate cultivated soil arising from different agronomic processes and plant K-uptake

Geoderma

Supplementary material

Eleanor Bakker[1,*]

Bruno Lanson[1,*]

Nathaniel Findling[1]

Michelle M. Wander[2]

Fabien Hubert[3]

(1) Univ. Grenoble Alpes, Univ. Savoie Mont Blanc, CNRS, IRD, IFSTTAR, ISTerre, F-38000 Grenoble, France

(2) Dept Natural Resources and Environmental Sciences, Univ. Illinois at Urbana-Champaign, Urbana, Illinois, USA

(3) Univ. Poitiers, CNRS, IC2MP, F-86000 Poitiers, France

* Corresponding author. E-mail: bruno.lanson@univ-grenoble-alpes.fr

Fig. S1. Grain size distributions obtained for all 1904-2014 soil samples with the sequential fractionation procedure described in the text. Size distribution are normalised to 100 %.

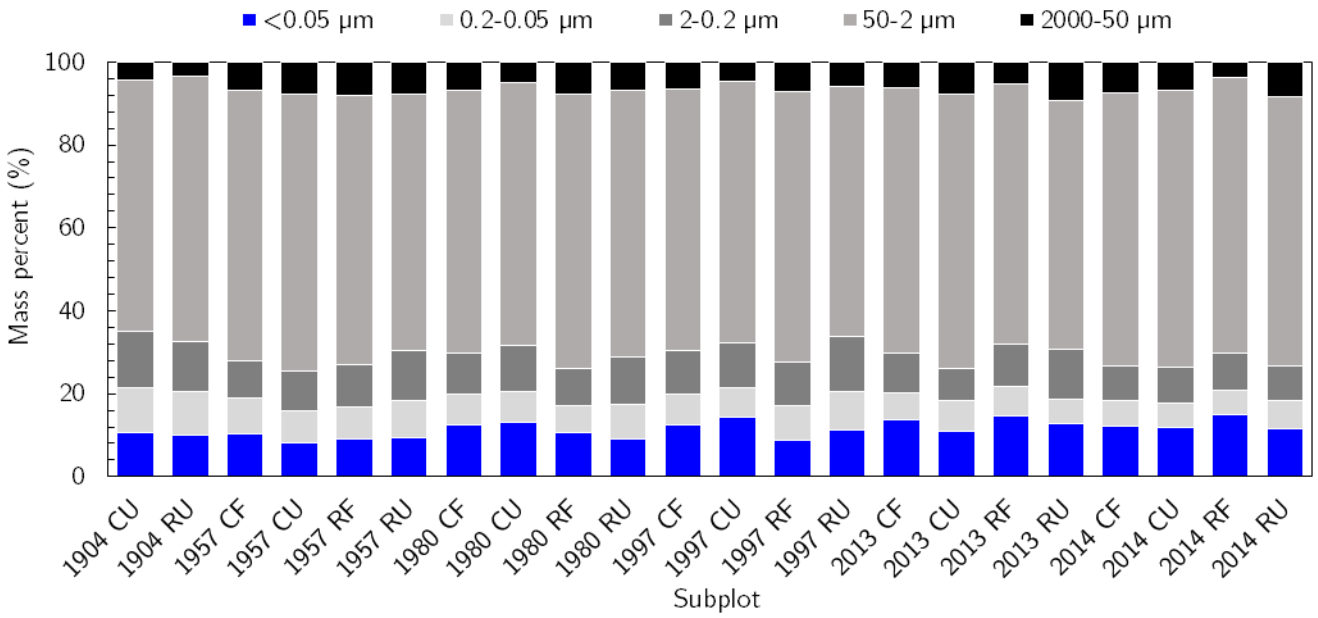

Fig. S2. Quantitative phase analysis performed with the Rietveld method on XRD patterns of samples 1904, 1957, 1980, 1997, 2013 and 2014. Experimental data is represented by black crosses, while solid red lines indicate the calculated intensity. Difference plots are solid grey lines underneath. a) CF subplots; b) CU subplots; c) RF subplots; d) RU subplots.

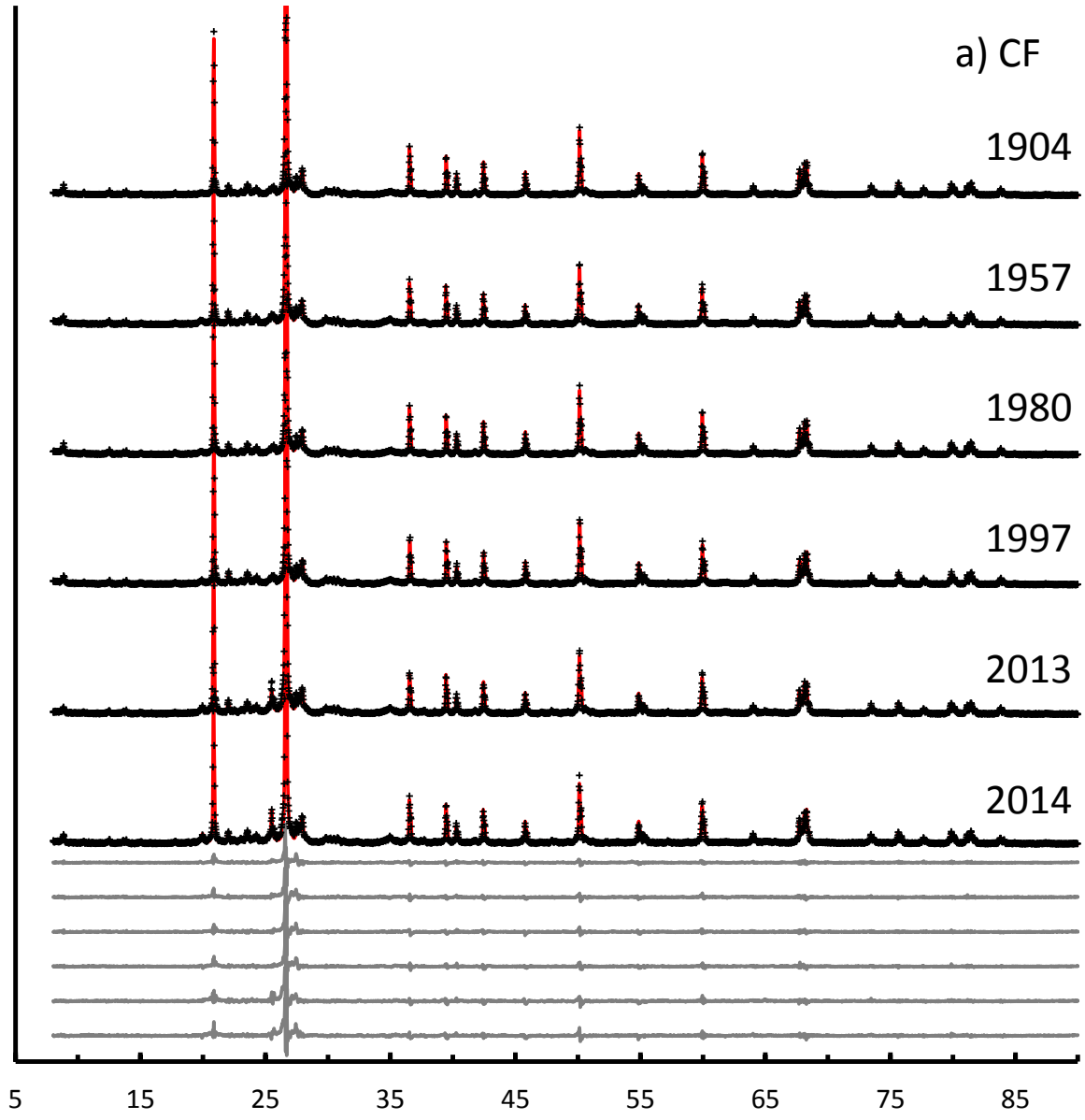

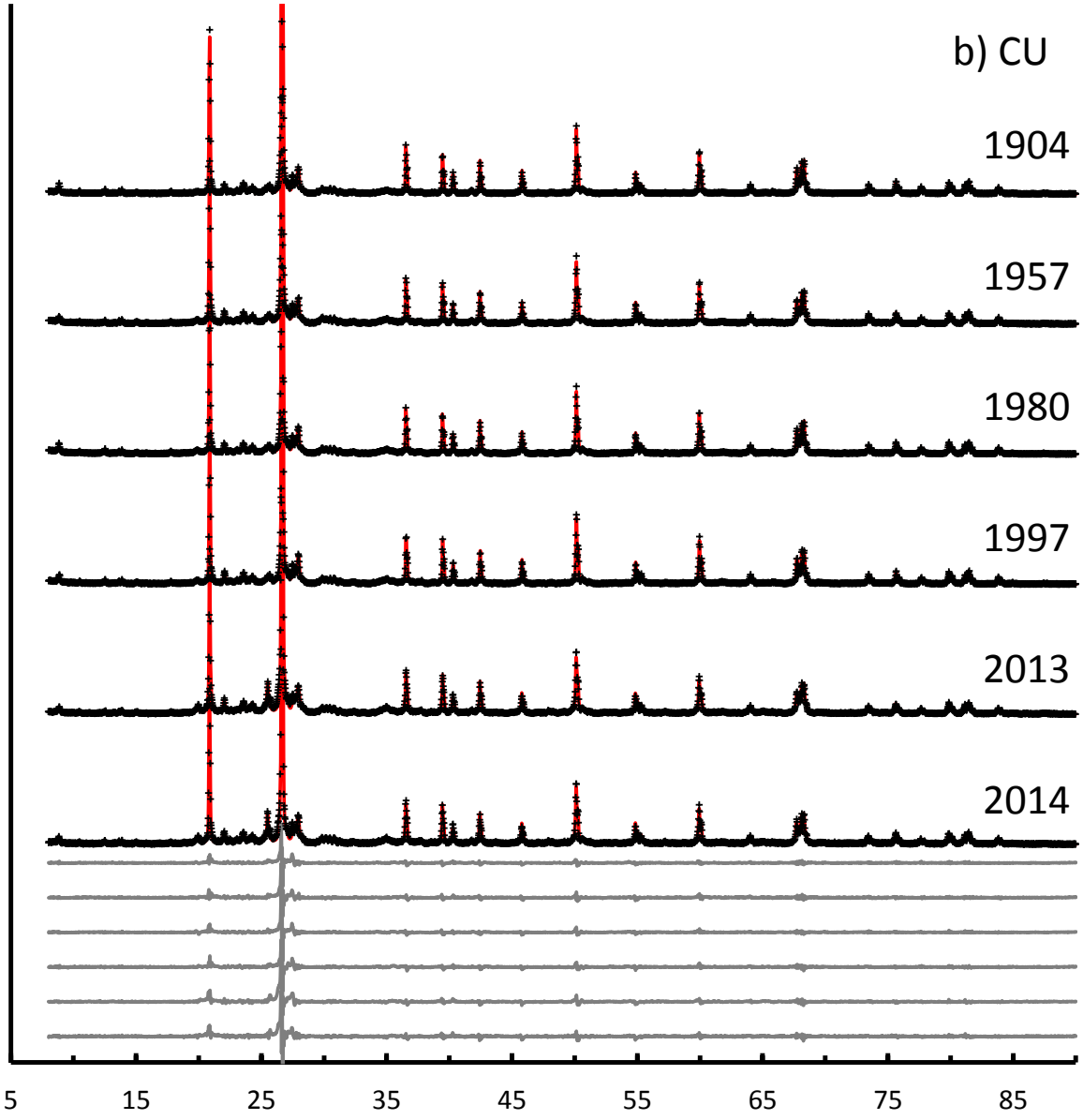
b) CU
1904
1957
1980
1997
2013
2014
5
15
25
35
45
55
65
75
85

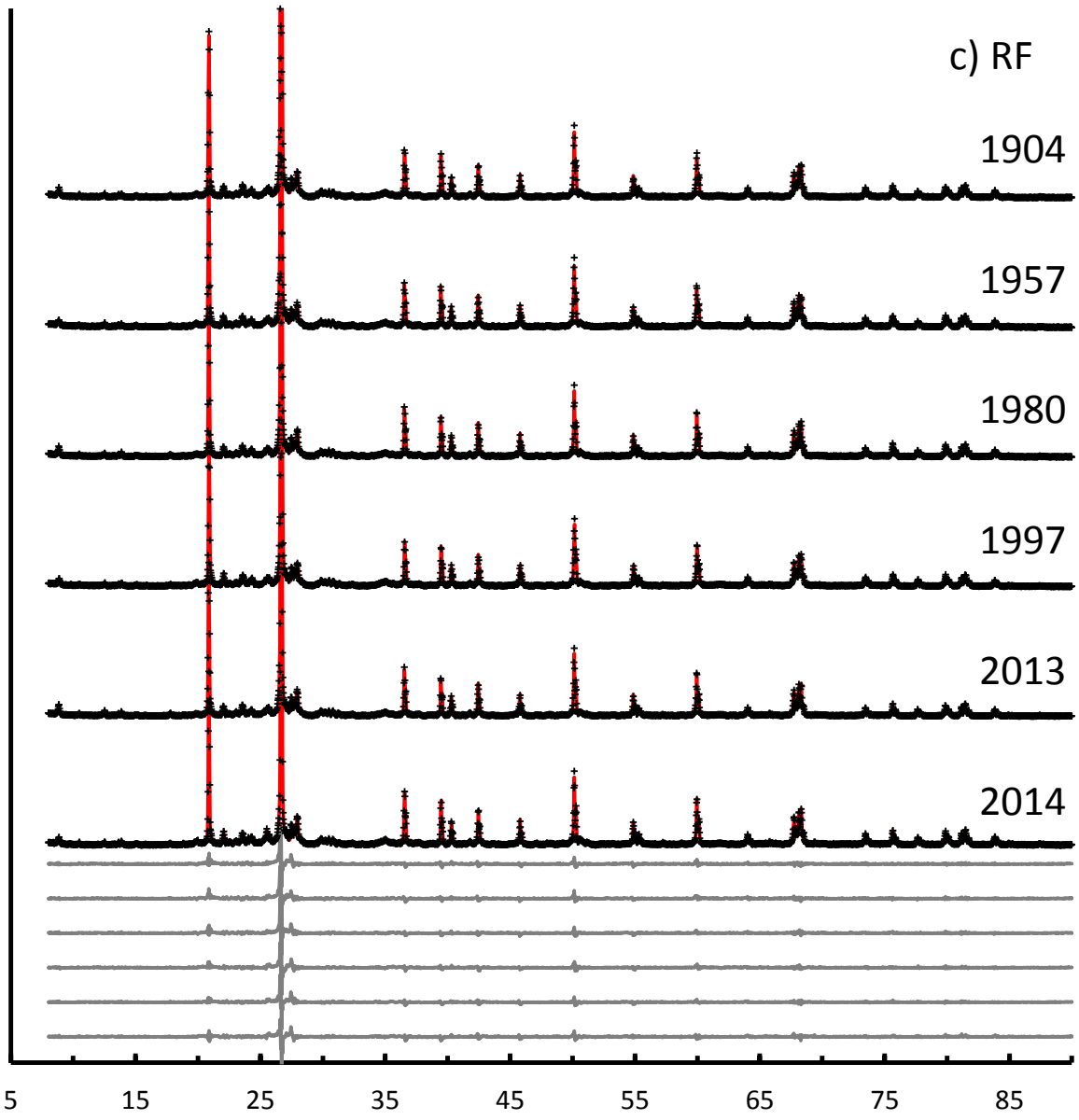
c) RF
1904
1957
1980
1997
2013
2014
5
15
25
35
45
55
65
75
85

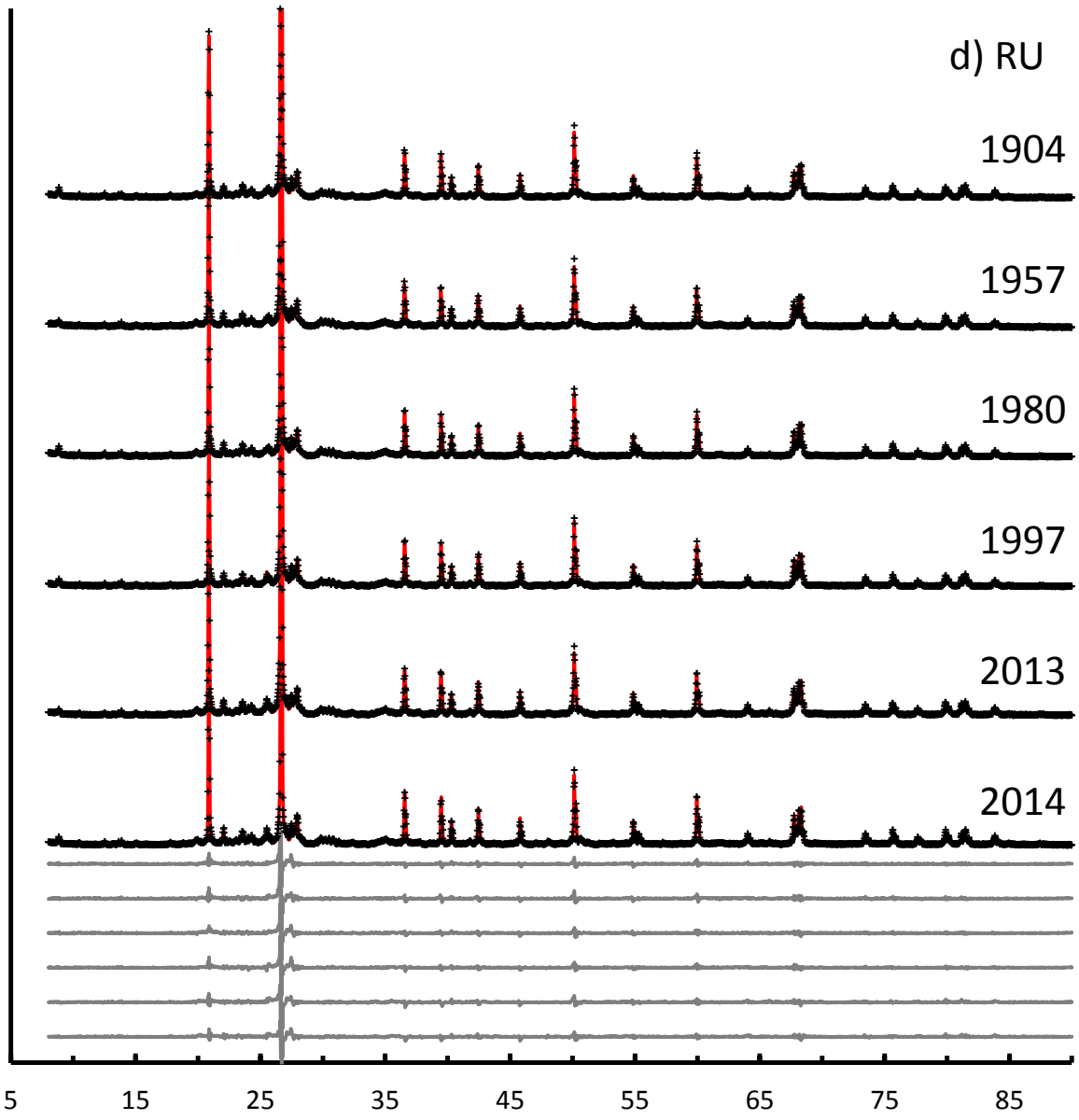
d) RU
1904
1957
1980
1997
2013
2014
5
15
25
35
45
55
65
75
85

Fig. S3. Comparison of experimental and calculated XRD patterns of the 2-0.2 µm clay subfraction (Ca-EG state). Experimental data is represented by black crosses, while solid red lines indicate the calculated intensity. Quartz, feldspar, and *hk* contributions from phyllosilicates are indicated by solid black, open black and solid grey triangles respectively. These contributions were not taken into account during the modelling procedure. The vertical grey bar represents an increase in intensity of the high-angle region compared to the 2–14° 2θ angular range. a) CF subplots; b) CU subplots; c) RF subplots; d) RU subplots.

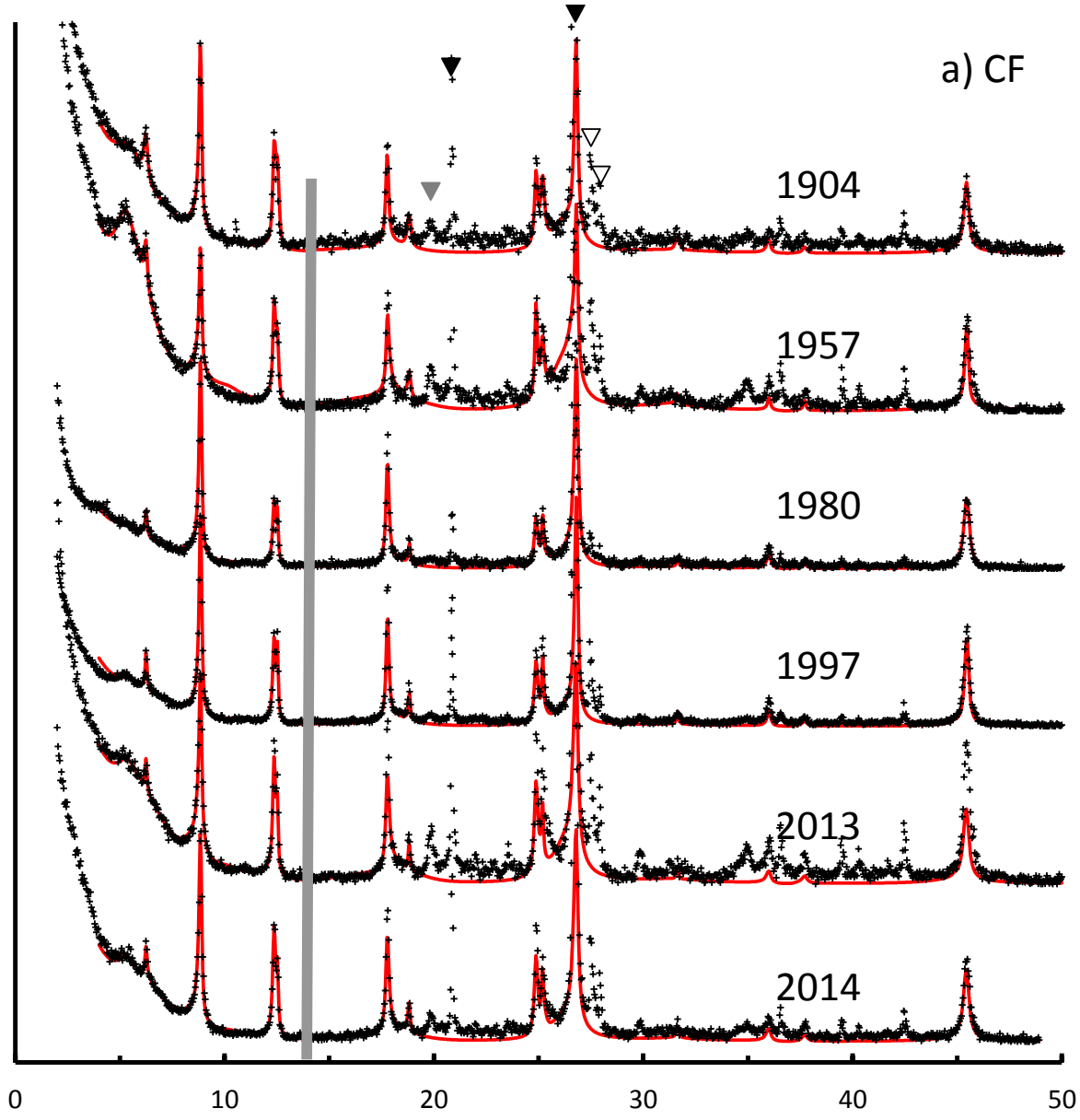

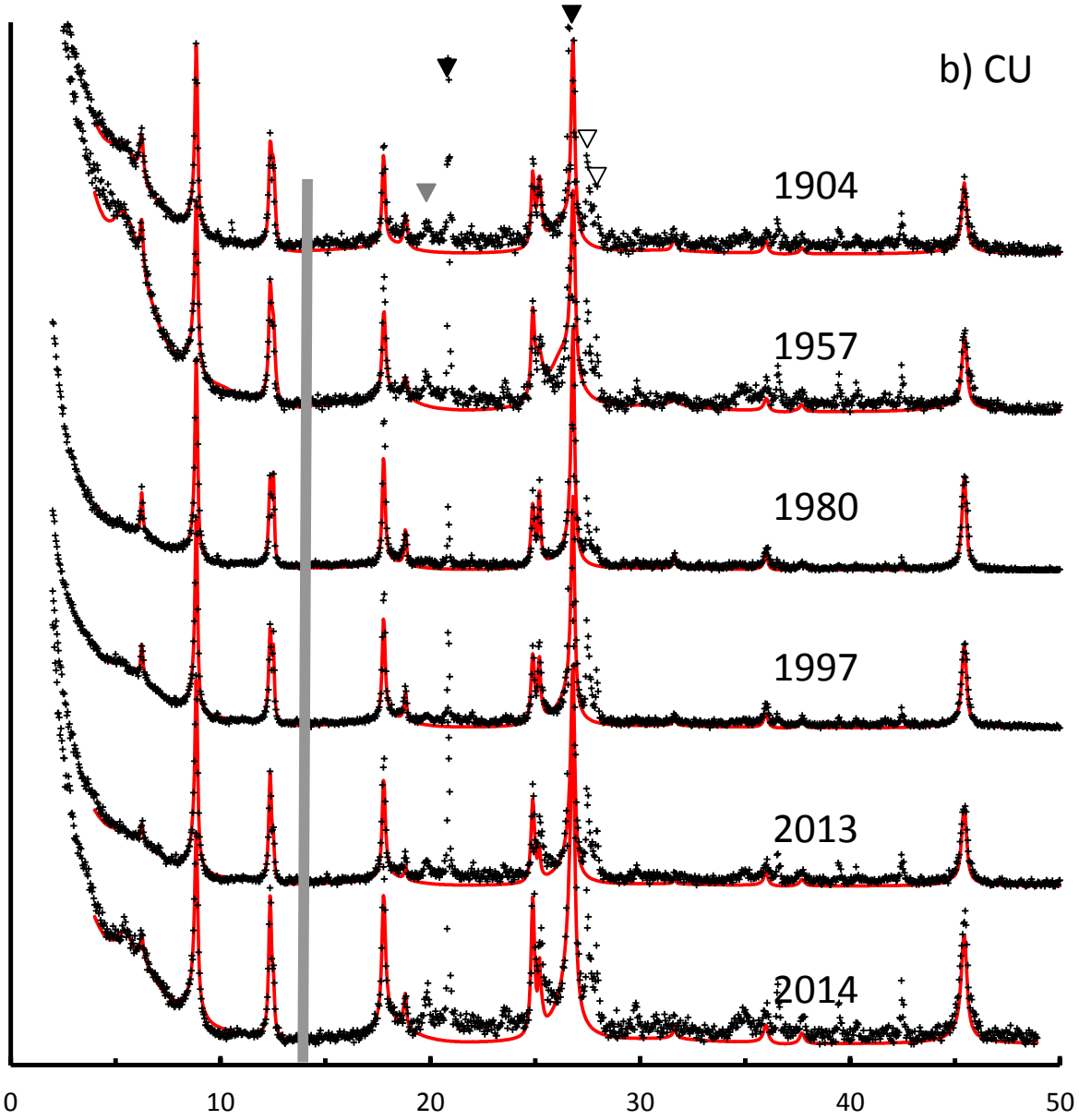
b) CU
1904
1957
1980
1997
2013
2014
0
10
20
30
40
50

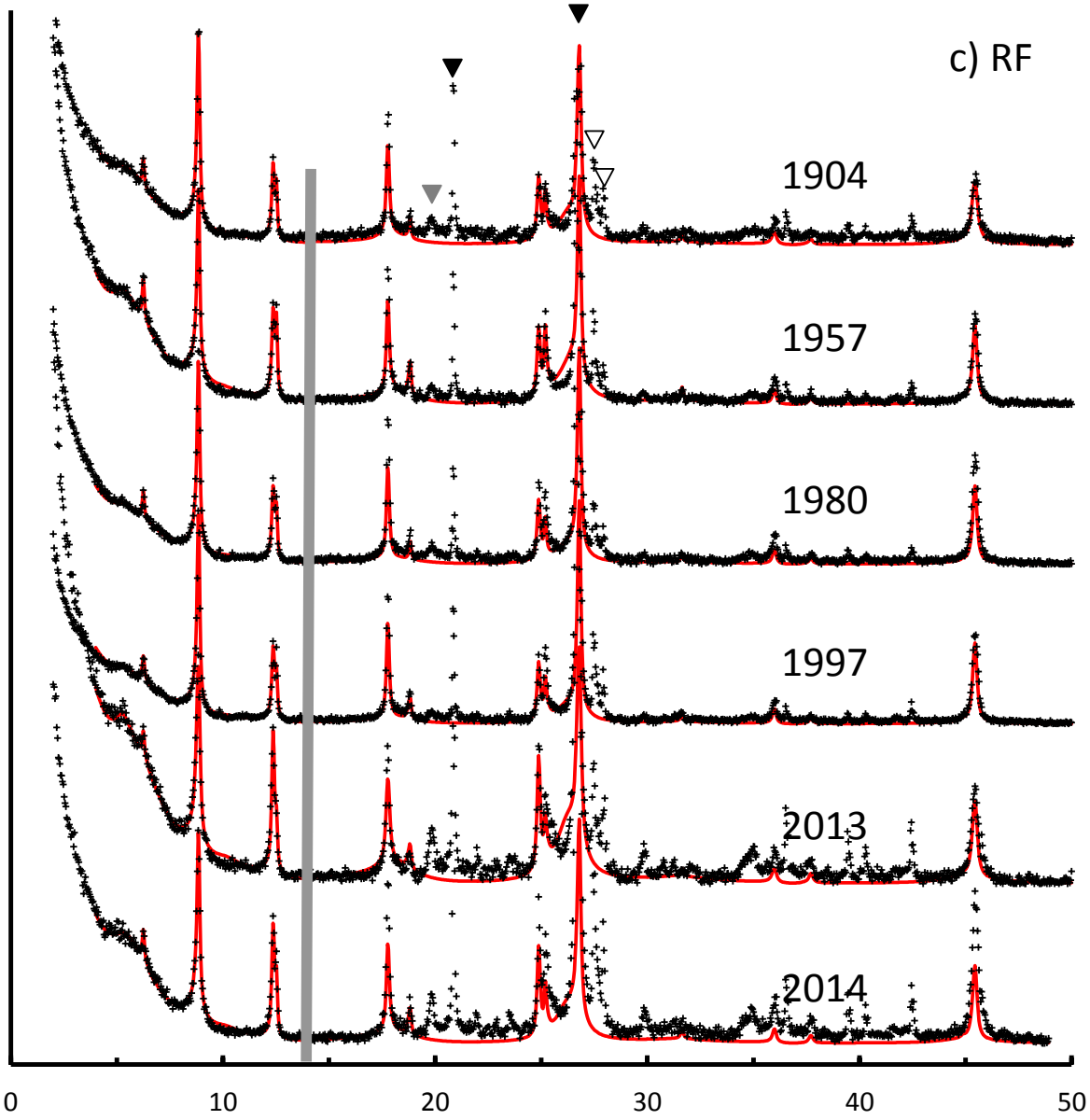
c) RF
1904
1957
1980
1997
2013
2014
0
10
20
30
40
50

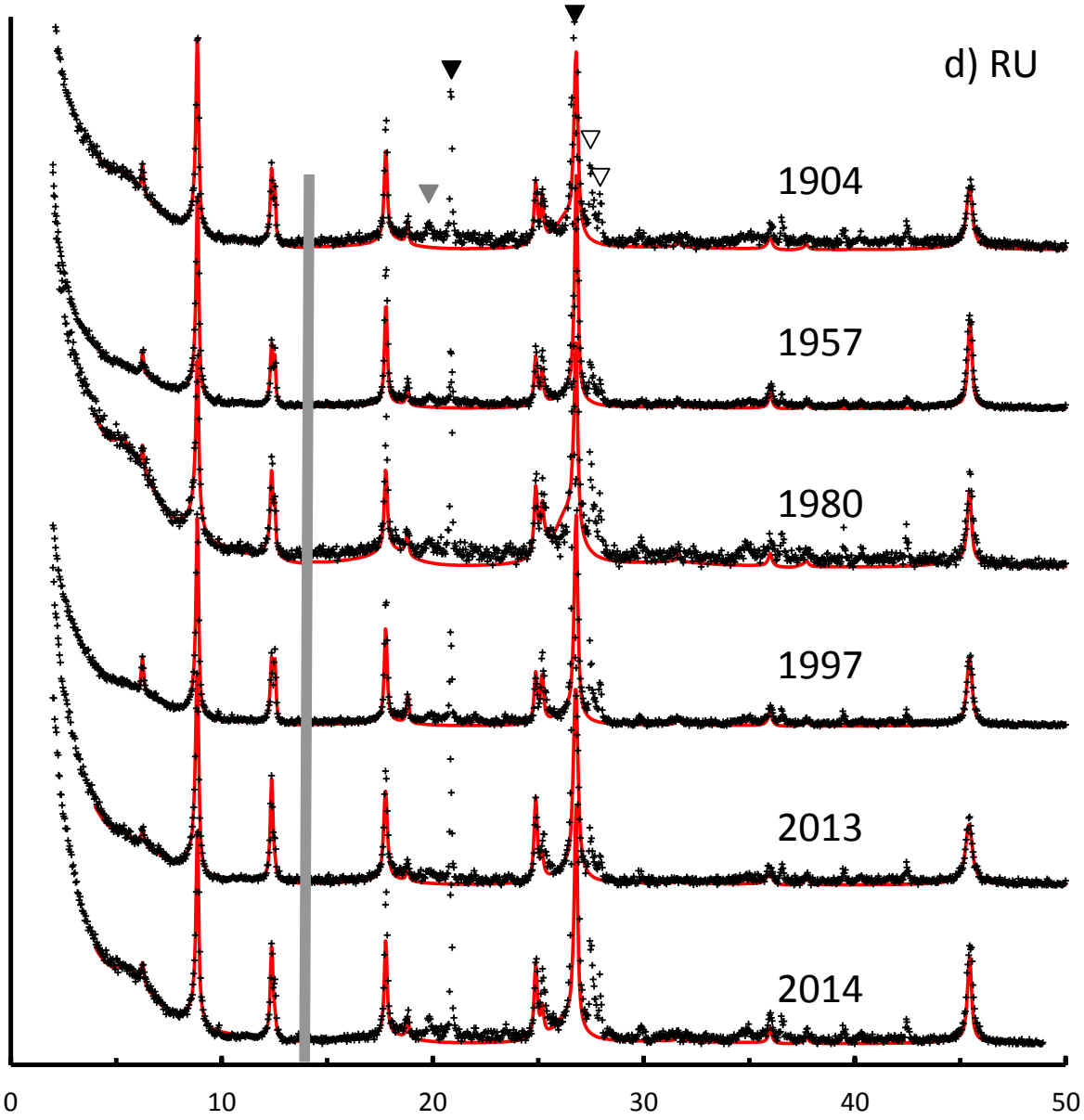
d) RU
1904
1957
1980
1997
2013
2014
0
10
20
30
40
50

Fig. S4. Comparison of experimental and calculated XRD patterns of the 0.2-0.05 µm clay subfraction (Ca-EG state). Experimental data is represented by black crosses, while solid red lines indicate the calculated intensity. Quartz, feldspar, and *hk* contributions from phyllosilicates are indicated by solid black, open black and solid grey triangles respectively. These contributions were not taken into account during the modelling procedure. The vertical grey bar represents an increase in intensity of the high-angle region compared to the 2–14° 2θ angular range. a) CF subplots; b) CU subplots; c) RF subplots; d) RU subplots.

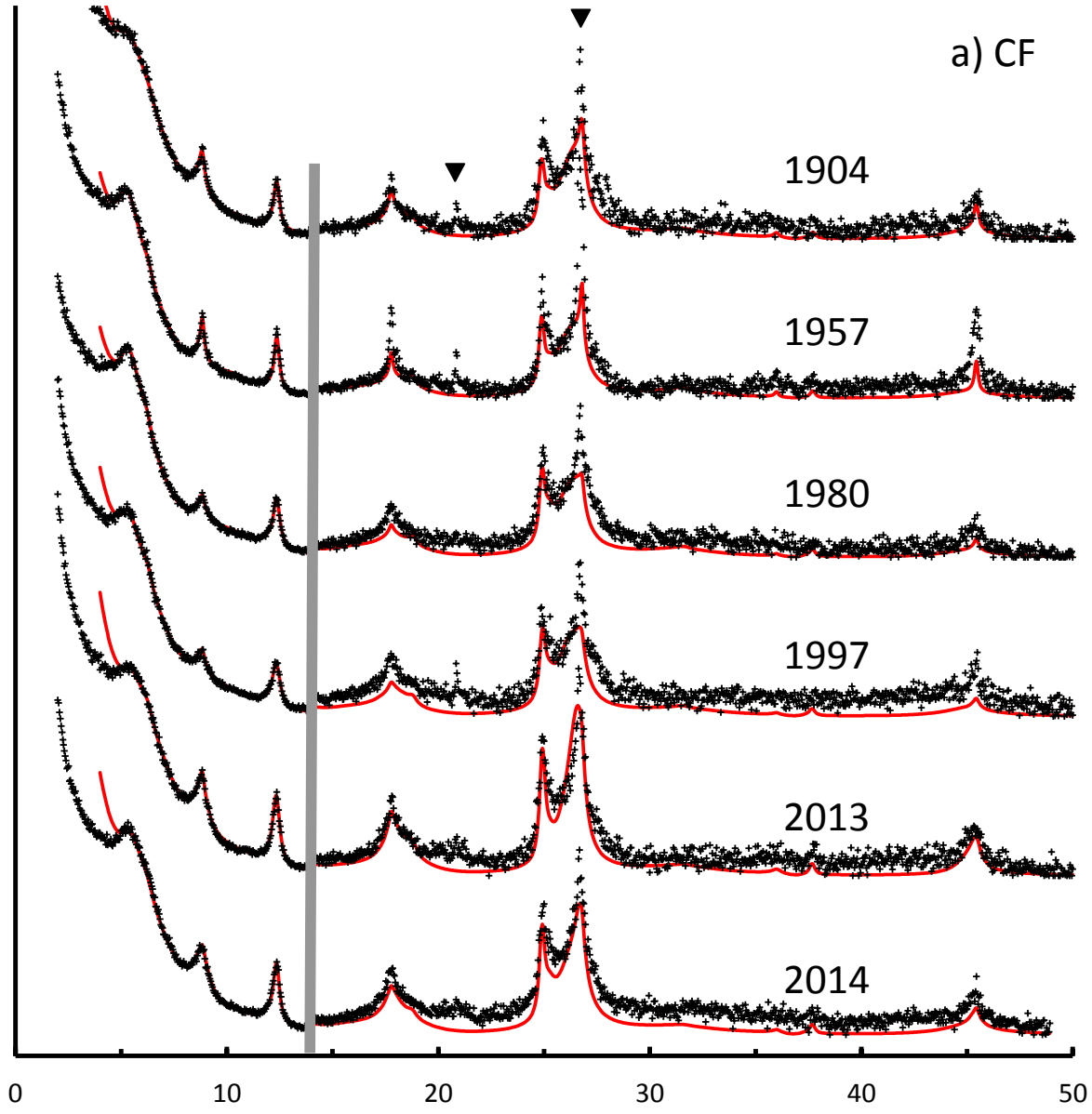

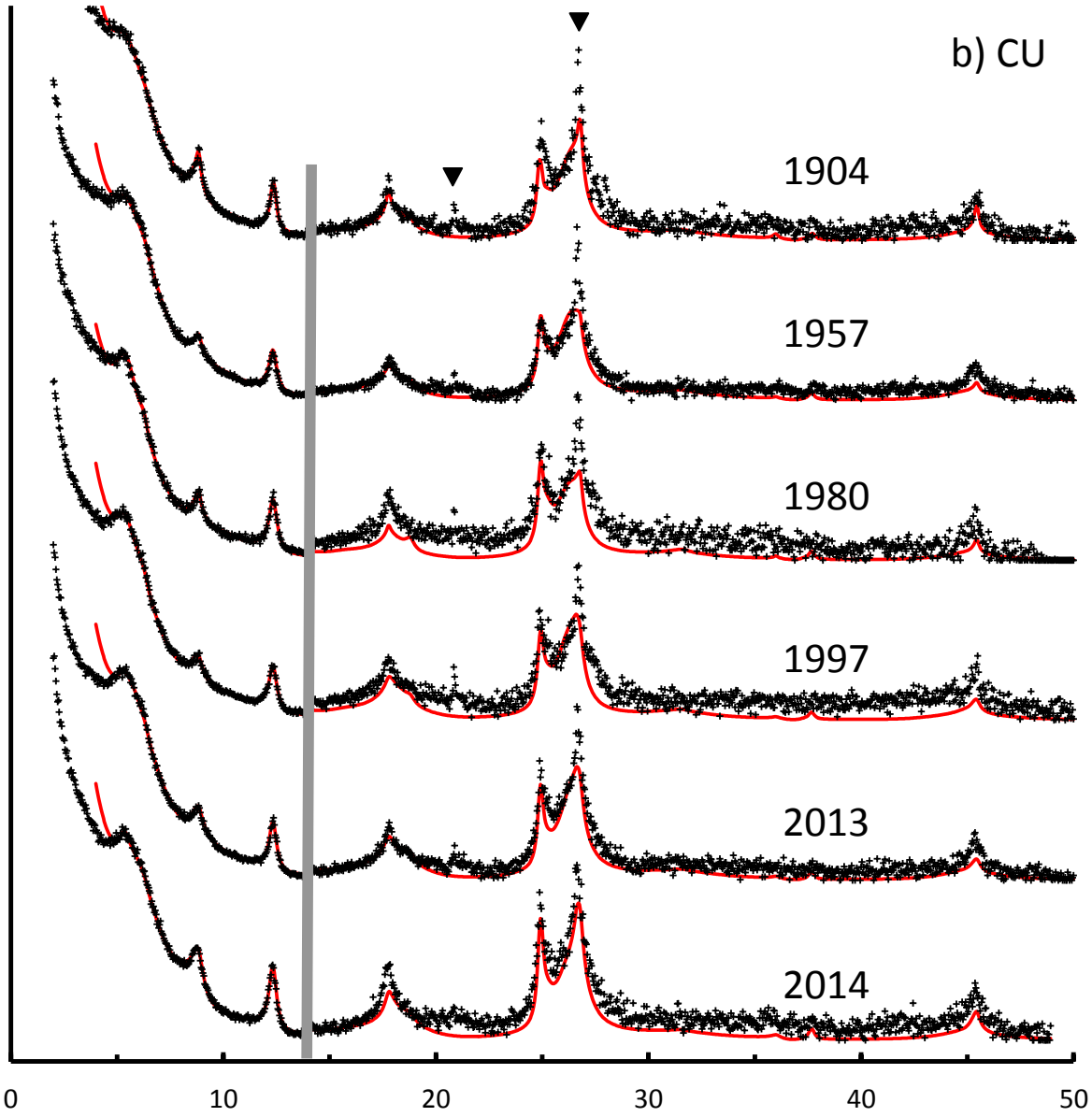
b) CU
1904
1957
1980
1997
2013
2014
0
10
20
30
40
50

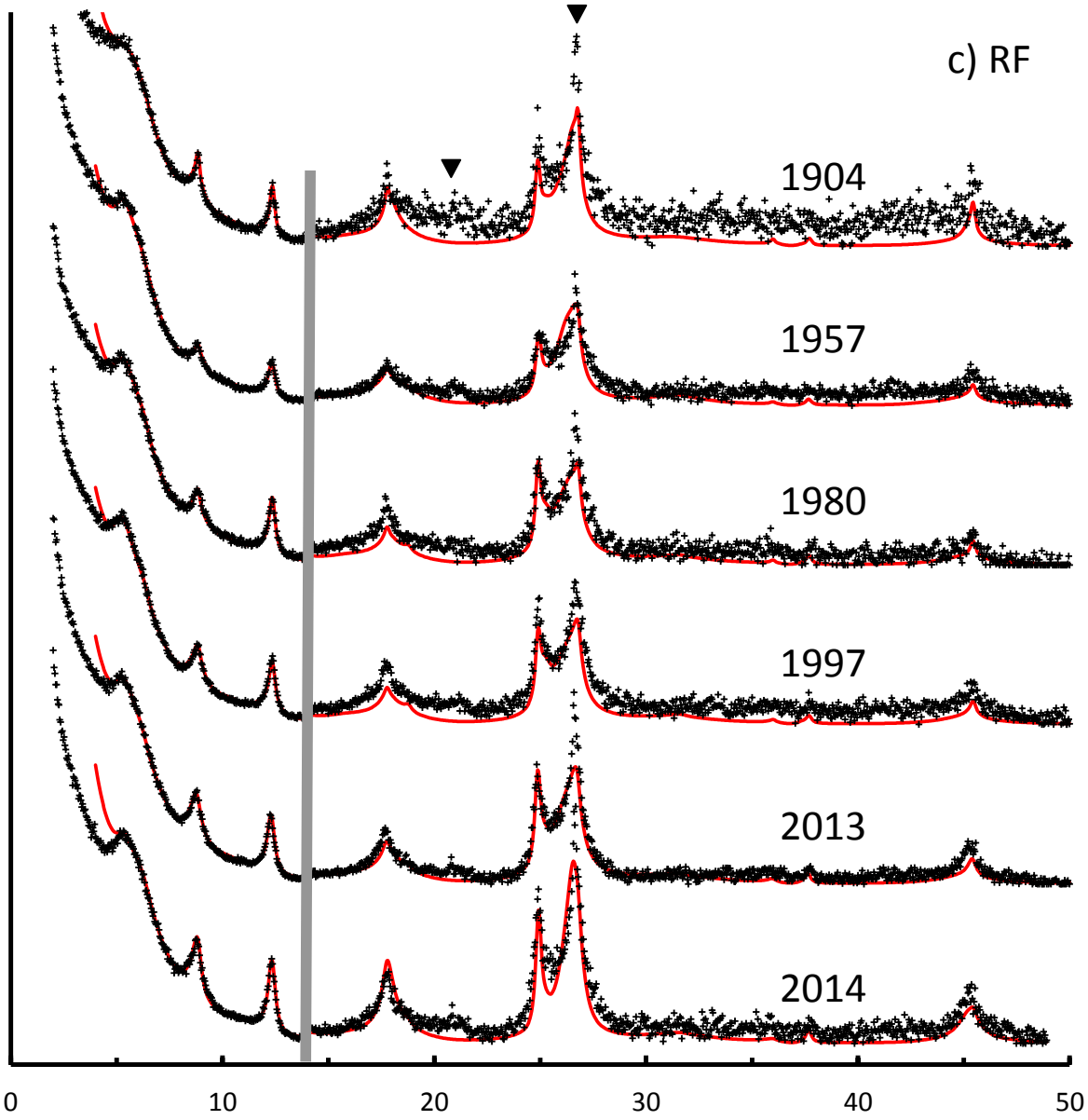
c) RF
1904
1957
1980
1997
2013
2014
0
10
20
30
40
50

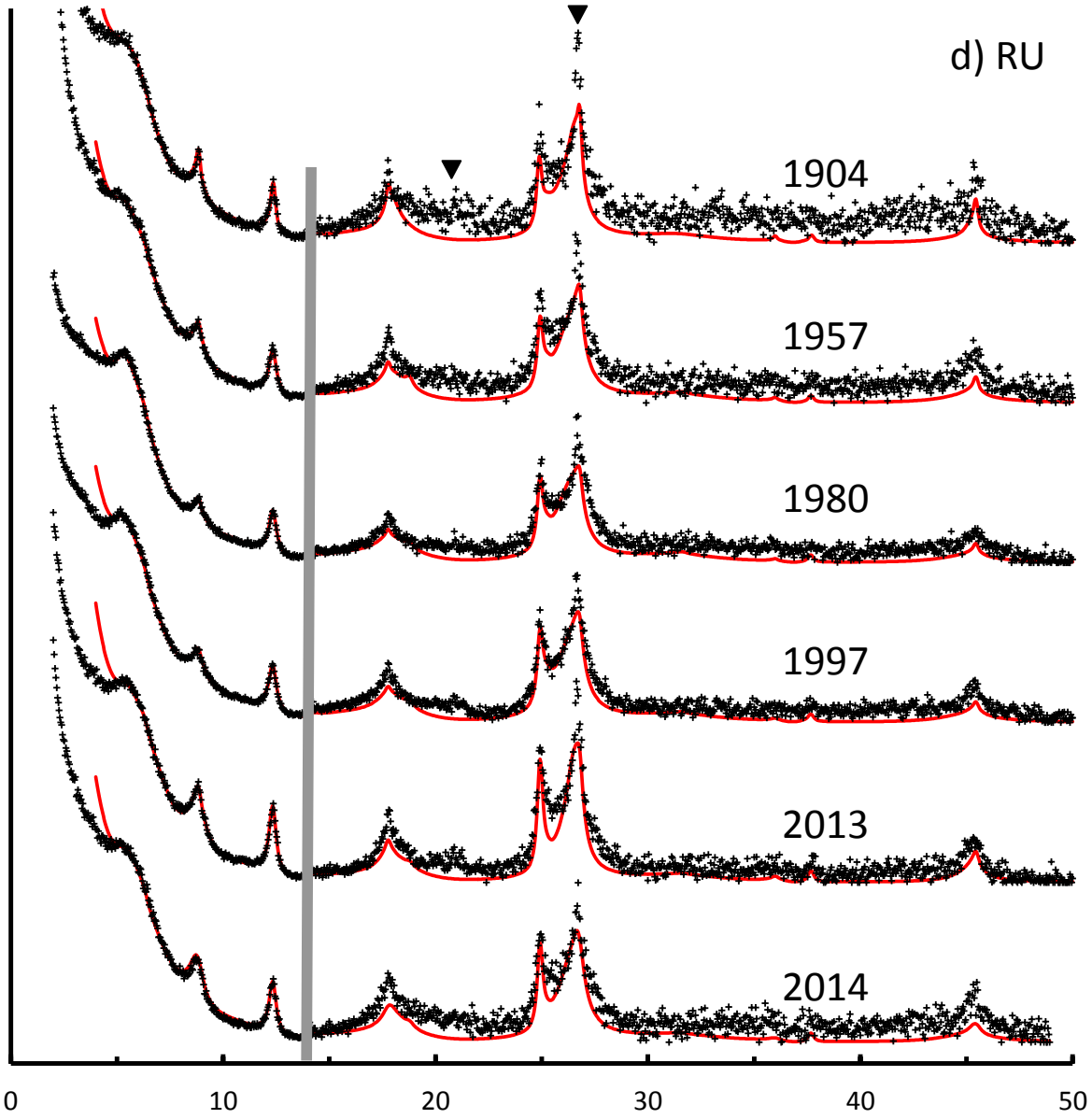
d) RU
1904
1957
1980
1997
2013
2014
0
10
20
30
40
50

Fig. S5. Comparison of experimental and calculated XRD patterns of the <0.05 µm clay subfraction (Ca-EG state). Experimental data is represented by black crosses, while solid red lines indicate the calculated intensity. Quartz, feldspar, and *hk* contributions from phyllosilicates are indicated by solid black, open black and solid grey triangles respectively. These contributions were not taken into account during the modelling procedure. The vertical grey bar represents an increase in intensity of the high-angle region compared to the 2–14° 2θ angular range. a) CF subplots; b) CU subplots; c) RF subplots; d) RU subplots.

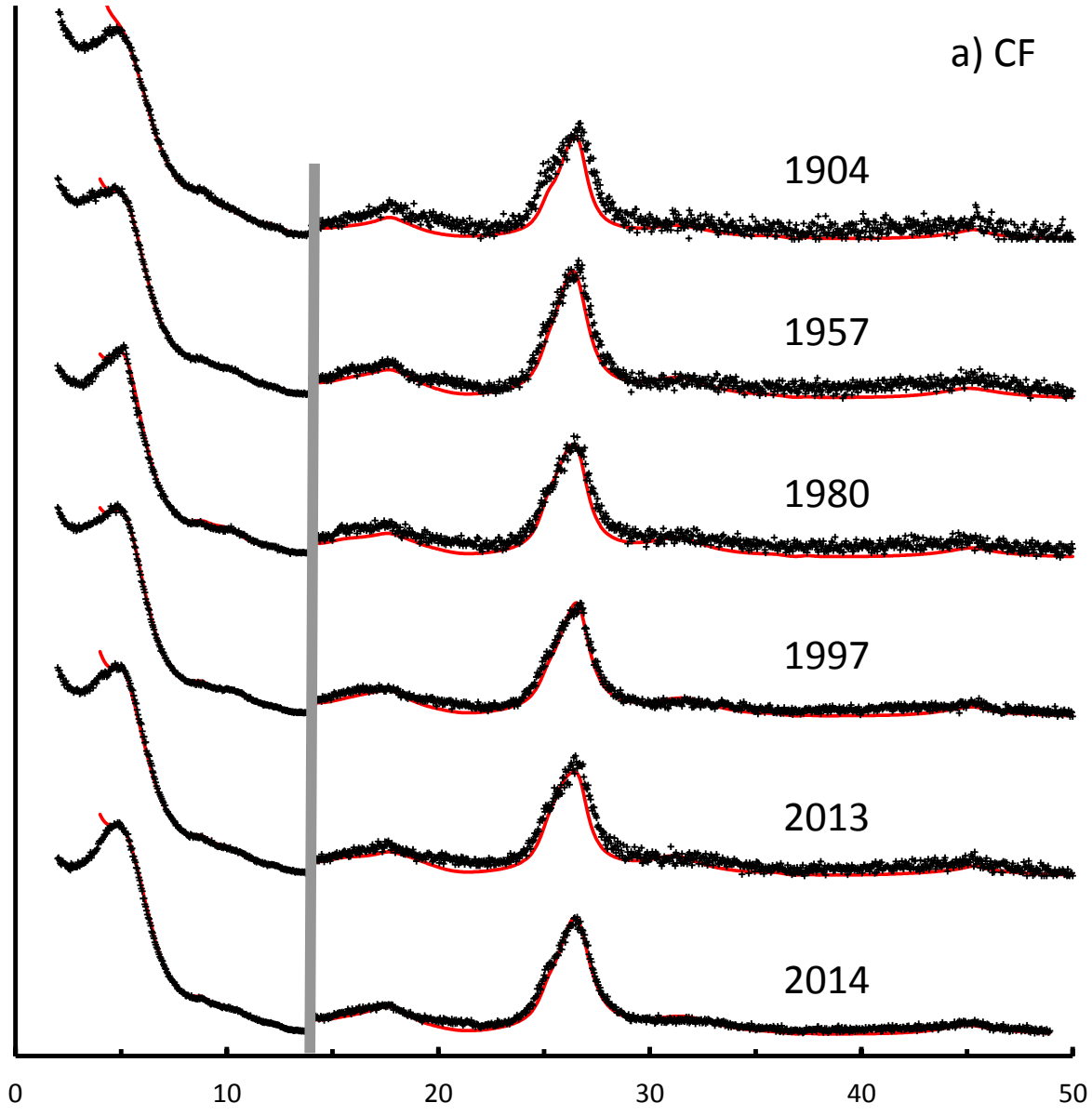

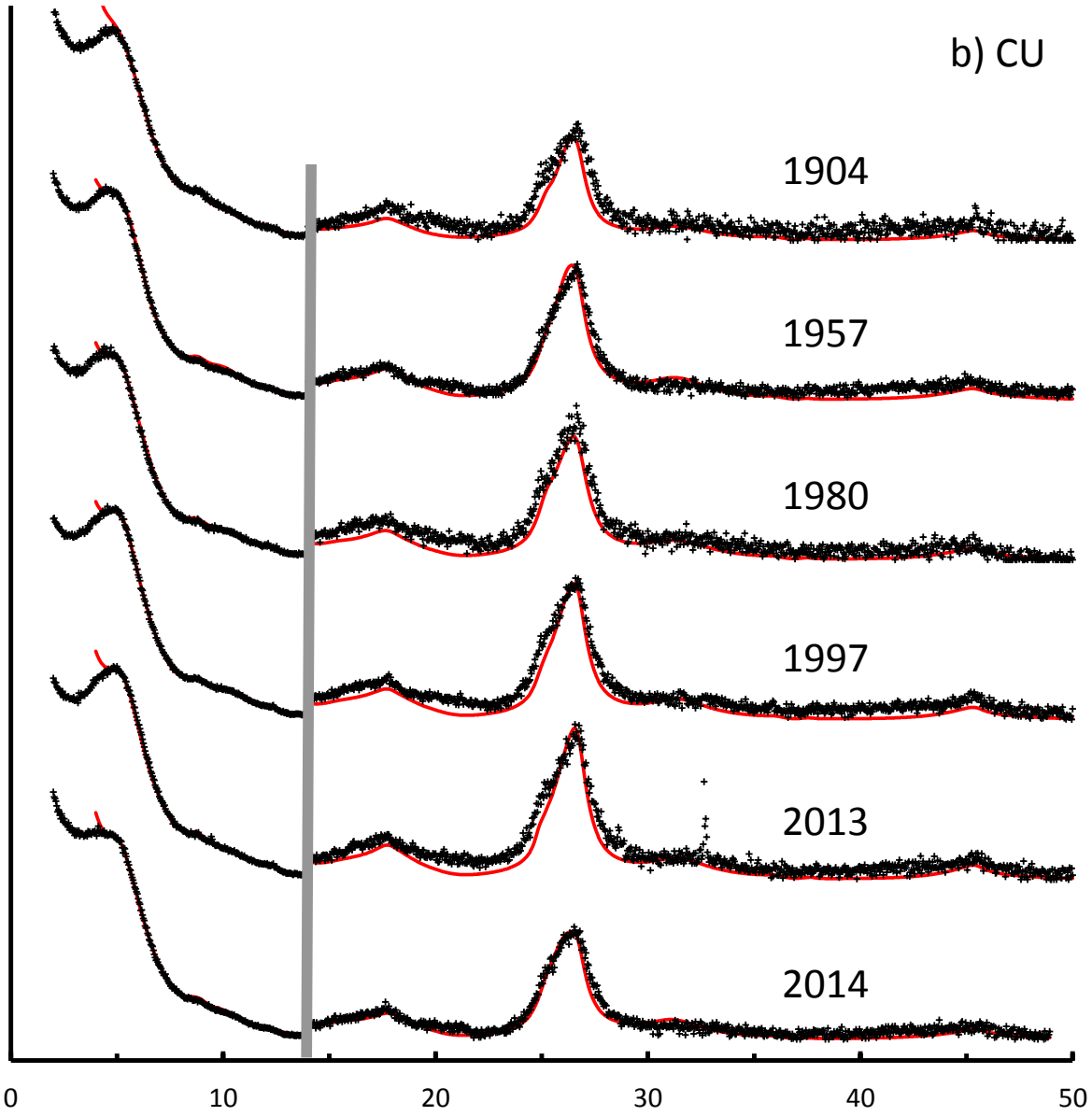
b) CU
1904
1957
1980
1997
2013
2014
0
10
20
30
40
50

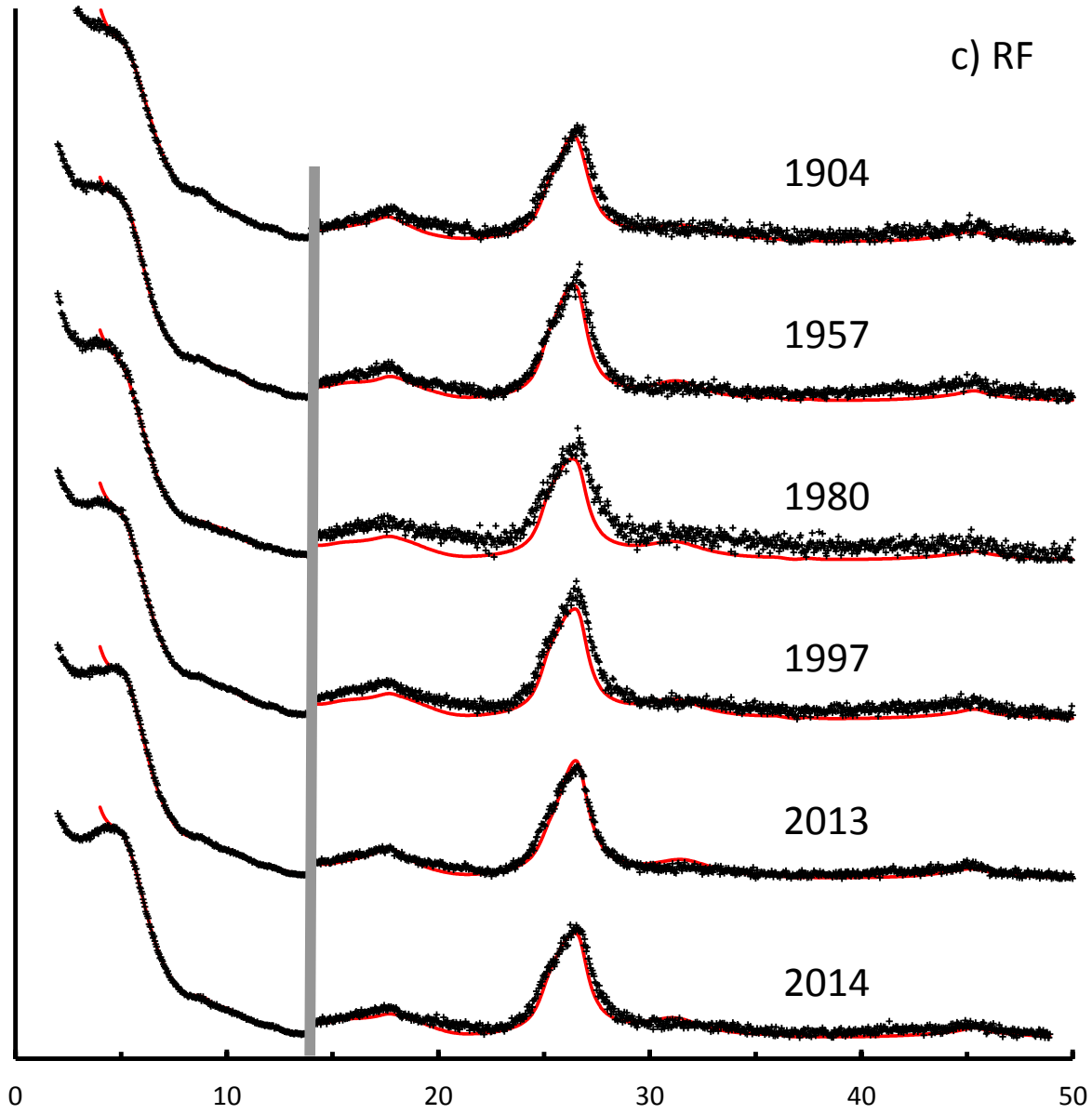
c) RF
1904
1957
1980
1997
2013
2014
0
10
20
30
40
50

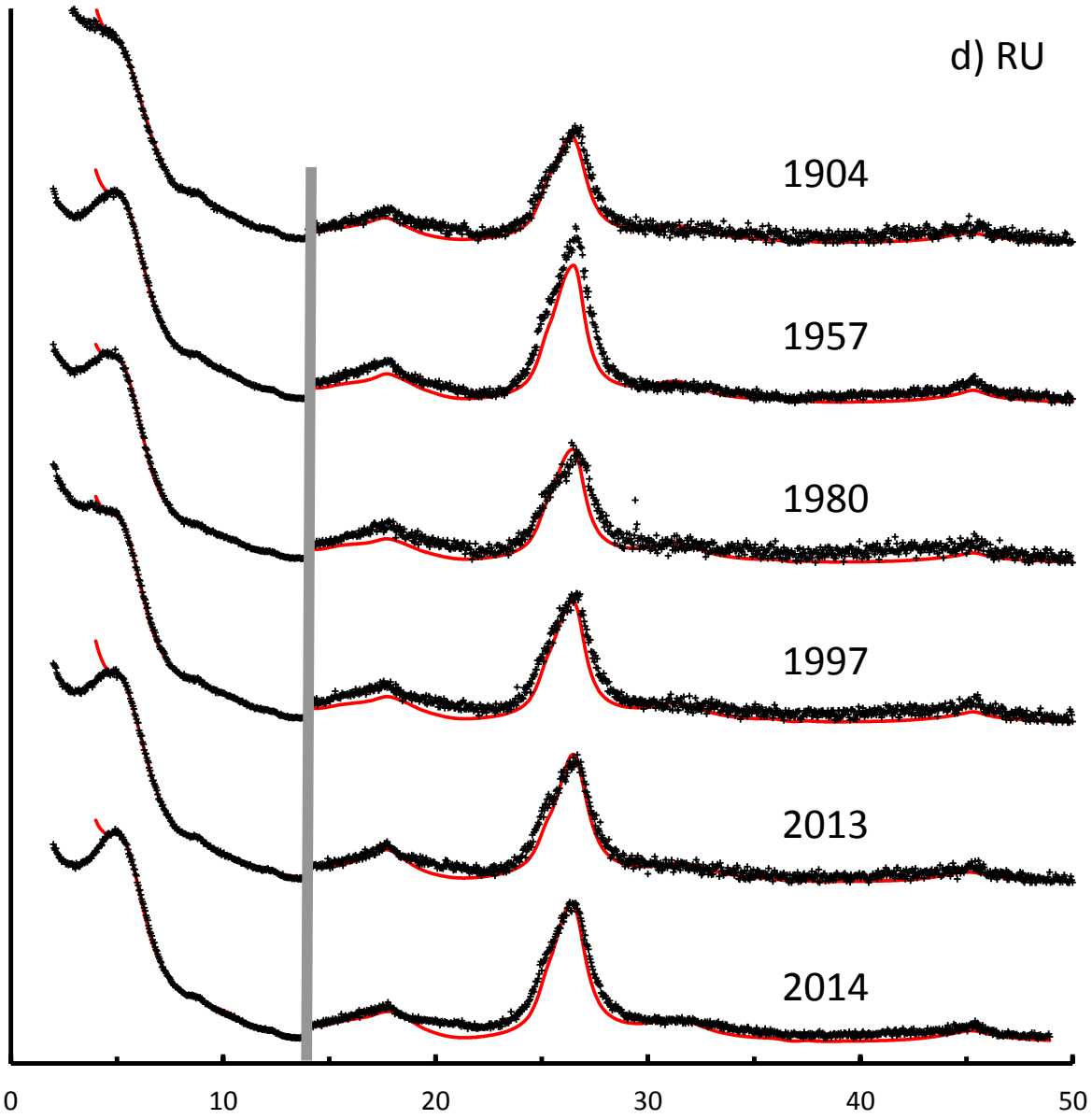
d) RU
1904
1957
1980
1997
2013
2014
0
10
20
30
40
50

Fig. S6. Relative abundances of illite, smectite, chlorite and kaolinite layers in the different clay subfractions (a: <0.05 µm, b: 0.2-0.05 µm, and c: 2-0.2 µm, c: 0.2-0.05 µm) and in the bulk <2 µm fraction (d). Yearly averages are represented by lines, symbols representing different agronomic practices. Smectite is represented in grey to enhance the difference between illite and smectite. Note the y-axis scale in d) is twice that of the other plots.

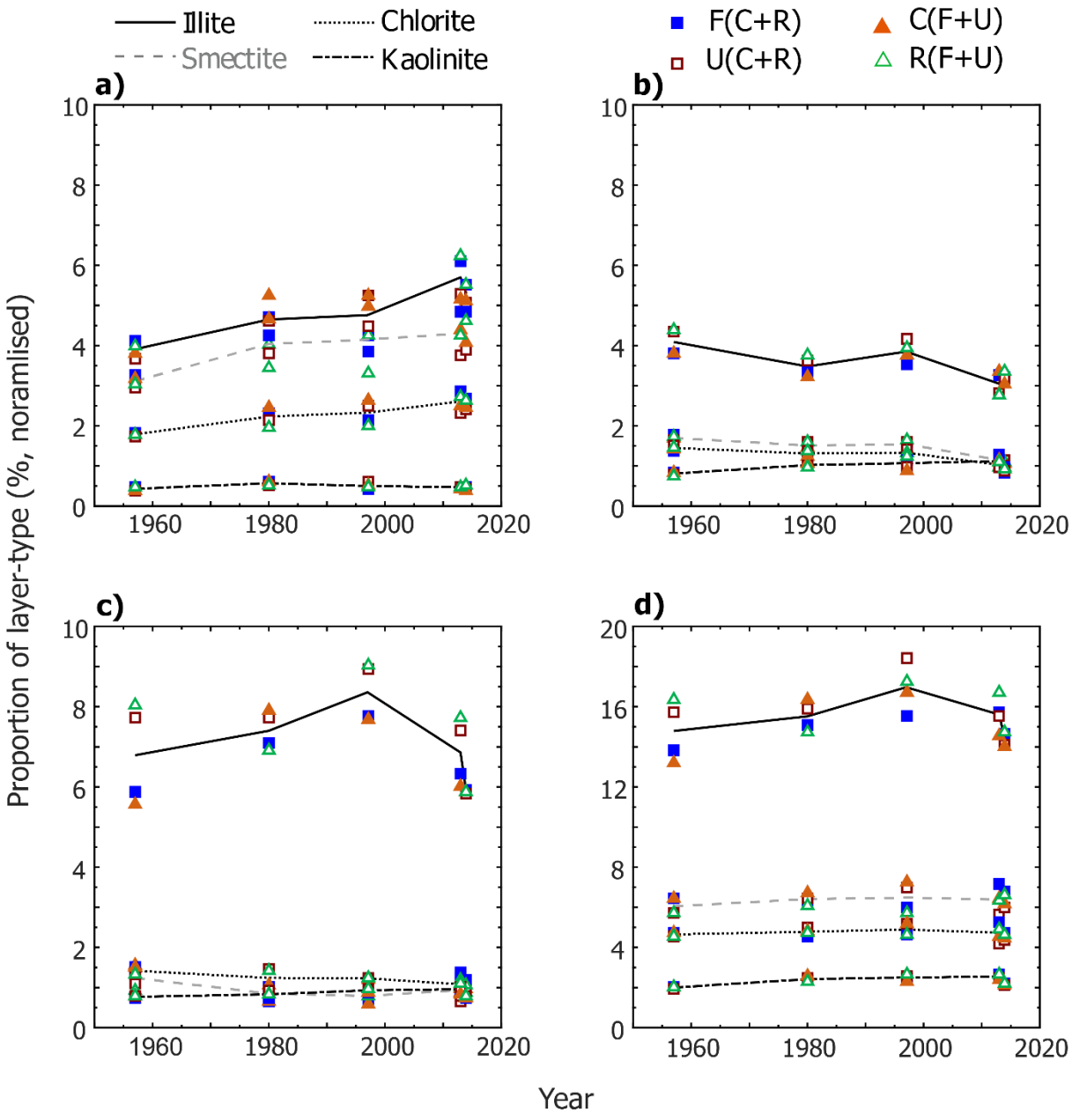

Table S1.

Relative proportions of the different mineral phases obtained from the modelling of experimental XRD patterns of the 50-2 µm fraction for 1904-2014 samples RU and CF subplots.

Mineral / Mineral group	1904 RU	1957 RU	1980 RU	1997 RU	2013 RU	2014 RU
Albite	11.1(3)	11.5(2)	10.3(3)	10.4(2)	10.1(4)	11.0(3)
Anatase	0.3(0)	0.6(1)	0.5(1)	0.8(1)	0.9(1)	1.0(1)
Calcite	0.4(0)	0.2(0)	0.3(0)	0.3(0)	0.2(0)	0.3(0)
Chlorite	1.7(2)	1.7(1)	1.8(2)	1.8(2)	1.1(2)	1.2(2)
Hornblende	0.6(1)	0.8(1)	0.8(1)	0.7(1)	0.6(1)	0.6(1)
Kaolinite	1.1(1)	1.0(1)	1.1(1)	1.1(1)	0.8(1)	0.3(1)
Microcline	12.0(3)	12.4(3)	12.1(4)	11.6(3)	11.5(4)	11.7(3)
Mica	4.8(2)	4.8(4)	5.6(18)	5.4(5)	4.9(26)	4.4(9)
Quartz	68.3(3)	67.0(4)	67.6(13)	68.8(5)	69.9(19)	69.5(7)
	1904 CU	**1957 CF**	**1980 CF**	**1997 CF**	**2013 CF**	**2014 CF**
Albite	10.1(2)	11.3(2)	10.9(2)	10.4(3)	12.2(2)	11.8(2)
Anatase	0.4(0)	0.3(0)	0.3(0)	0.3(1)	1.0(1)	1.3(1)
Calcite	0.3(0)	0.3(0)	0.2(0)	0.3(0	0.3(1)	0.3(1)
Chlorite	1.4(1)	1.6(2)	2.1(2)	2.0(2)	2.0(2)	1.6(2)
Hornblende	0.9(1)	0.6(1)	0.7(1)	0.7(1)	0.6(1)	0.6(1)
Kaolinite	1.2(2)	1.4(1)	1.2(1)	1.2(1)	0.9(1)	1.2(1)
Microcline	10.7(2)	10.4(3)	11.8(3)	10.2(4)	11.3(3)	10.8(3)
Mica	4.1(2)	5.4(14)	4.6(11)	6.4(23)	5.7(3)	6.4(3)
Quartz	71.1(3)	68.7(11)	68.2(9)	68.5(17)	66.0(4)	65.9(4)

Table S2a

Relative proportions (wt %) and compositions of the different mineral phases used to fit experimental XRD patterns of the 2-0.2 µm subfractions for 1904-2014 samples (RU and RF subplots). Values are given for composition in the Ca-EG state.

Contribution Ab. (%) / Comp.	1904 RU	1957 RU	1980 RU	1997 RU	2013 RU	2014 RU
Illite	42	53	26	51	56	51
ISSCh 90	8	12 94/1/5	13 94/1/5	12 92/4/5	13 92/3/5	8 92/3/5
ISSCh 80	10 80/6/14	9 75/11/14	6 78/10/12	4 75/11/14	5 75/11/14	11 75/11/14
ISSCh 50	21 55/20/25	14 45/20/25	27 50/25/25	16 50/25/25	10 50/25/25	15 50/25/25
ISSCh 35	7 35/45/20	1 35/45/20	10 35/45/20	1 35/45/20	1 35/45/20	2 35/45/20
ISSCh 5	<1 0/80/20	<1 0/80/20	<1 0/80/20	<1 0/80/20		<1 0/80/20
Kaolinite	5	5	8	7	10	8
KI R1	3	2	6	5	3	3
Chlorite	3	3	4	4	2	2
ICh 6	1 10/90	1 10/90	10/90		1/99	1/99
Smectite						
		1957 RF	**1980 RF**	**1997 RF**	**2013 RF**	**2014 RF**
Illite		31	44	45	29	41
ISSCh 90		9 94/1/5	16 94/1/5	14 94/1/5	15 94/1/5	13 94/1/5
ISSCh 80		17 78/8/14	8 76/10/12	5 78/10/12	5 78/12/10	7 78/12/10
ISSCh 50		22 45/30/25	12 45/30/25	19 50/25/25	27 50/25/25	14 50/25/25
ISSCh 35		7 35/45/20	4 35/45/20	2 35/45/20	6 35/45/20	7 35/45/20
ISSCh 5		<1 0/80/20	<1 0/80/20	<1 0/80/20	1 0/80/20	2 0/80/20
Kaolinite		5	8	7	7	8
KI R1		3	5	5	8	5
Chlorite		4	3	3	2	3
ICh 6		2 10/90	10/90	10/90	10/90	10/90
Smectite						

Table S2b

Relative proportions (wt %) and compositions of the different mineral phases used to fit experimental XRD patterns of the 0.2-0.05 µm subfractions for 1904-2014 samples (RU and RF subplots). Values are given for composition in the Ca-EG state.

Contribution Ab. (%) / Comp.	1904 RU	1957 RU	1980 RU	1997 RU	2013 RU	2014 RU
Illite	6	4	3	2	3	1
ISSCh 90	7 94/2/4	14 90/6/4	12 90/6/4	14 90/6/4	20 91/5/4	19 94/2/4
ISSCh 80	22 80/6/14	9 75/11/14	9 70/16/14	12 70/16/14	14 75/12/14	12 75/8/14
ISSCh 50	33 55/20/25	44 54/21/25	44 52/23/25	42 52/23/25	35 50/25/25	41 52/23/25
ISSCh 35	19 35/45/20	16 35/45/20	17 30/50/20	14 30/50/20	12 30/50/20	14 30/50/20
ISSCh 5	1 10/70/20	2 10/70/20	2 5/75/20	1 0/80/20	1 0/80/20	1 0/80/20
Kaolinite	5	6	7	6	10	9
KI R1 Chlorite	7	3	5	8	4	3
ICh 6 Smectite	0 6/94	2 6/94	1 3/97	1 3/97	1 3/97	1 3/97
		1957 RF	**1980 RF**	**1997 RF**	**2013 RF**	**2014 RF**
Illite		3	4	3	2	3
ISSCh 90		11 90/6/4	8 94/3/3	12 94/3/3	13 95/1/4	12 96/1/3
ISSCh 80		8 75/11/14	15 78/08/14	13 78/8/14	13 78/8/14	16 75/11/14
ISSCh 50		43 54/21/25	33 53/22/25	33 53/22/25	35 54/21/25	33 52/23/25
ISSCh 35		22 35/45/20	20 35/45/20	17 35/45/20	14 32/48/20	15 32/48/20
ISSCh 5		2 0/80/20	2 0/80/20	2 0/80/20	1 5/75/20	2 5/75/20
Kaolinite		6	7	7	15	9
KI R1 Chlorite		5	10	12	7	9
ICh 6 Smectite		1 3/97	1 6/94	1 6/94	1 6/94	1 6/94

Table S2c

Relative proportions (wt %) and compositions of the different mineral phases used to fit experimental XRD patterns of the <0.05 µm subfractions for 1904-2014 samples (RU and RF subplots). Values are given for composition in the Ca-EG state.

Contribution Ab. (%) / Comp.	1904 RU	1957 RU	1980 RU	1997 RU	2013 RU	2014 RU
Illite						
ISSCh 90	13 89/8/3	13 89/7/4	11 89/4/7	11 89/6/4	12 89/6/4	9 89/6/4
ISSCh 80						
ISSCh 50	38 55/23/22	36 54/24/22	34 54/24/22	38 54/24/22	43 54/24/22	40 54/24/22
ISSCh 35	38 40/34/26	39 30/44/26	40 30/44/26	38 30/44/26	36 33/41/26	39 30/44/26
ISSCh 5	4 0/80/8/12	5 0/88/12	8 0/88/12	5 0/88/0/12	3 0/88/12	5 0/88/12
Kaolinite KI R1	6	6	6	6	5	5
Chlorite ICh 6						
Smectite	1	1	1	2	1	2
		1957 RF	**1980 RF**	**1997 RF**	**2013 RF**	**2014 RF**
Illite						
ISSCh 90		11 89/7/0/4	10 88/3/5/4	12 89/6/1/4	9 89/6/1/4	10 89/4/2/4
ISSCh 80						
ISSCh 50		36 54/23/22	38 52/26/22	40 50/28/22	42 54/24/22	36 50/28/22
ISSCh 35		38 30/44/26	40 35/39/26	36 30/44/26	39 33/44/26	42 30/44/26
ISSCh 5		6 0/88/12	5 0/88/12	6 0/88/12	5 0/88/12	6 0/88/12
Kaolinite KI R1		7	5	5	4	5
Chlorite ICh 6						
Smectite		2	2	1	1	1

Table S3a

Relative proportions (wt %) and compositions of the different mineral phases used to fit experimental XRD patterns of the 2-0.2 µm subfractions for 1904-2014 samples (CU and CF subplots). Values are given for composition in the Ca-EG state.

Contribution Ab. (%) / Comp.	1904 CU	1957 CU	1980 CU	1997 CU	2013 CU	2014 CU
Illite	40	26	48	39	44	38
ISSCh 90	6 92/3/5	11 94/0/6	11 95/0/5	14 95/0/5	18 95/0/5	14 92/2/6
ISSCh 80	6 80/6/14	10 75/11/14	9 75/11/14	6 75/11/14	6 75/11/14	8 75/11/14
ISSCh 50	24 50/25/25	27 45/30/25	10 45/30/25	20 45/30/25	14 42/33/25	19 42/33/25
ISSCh 35	7 40/40/20	12 35/45/20	2 35/45/20	4 35/45/20	2 35/45/20	4 30/50/20
ISSCh 5	<1 0/80/20	1 0/80/20	<1 0/80/20	<1 0/80/20	0 0/80/20	<1 0/80/20
Kaolinite	6	5	9	8	11	10
KI R1	5	4	5	6	3	4
Chlorite	6	4	6	3	2	3
ICh 6						
Smectite						

	1957 CF	1980 CF	1997 CF	2013 CF	2014 CF
Illite	19	53	47	28	48
ISSCh 90	11 92/0/8	10 95/0/5	10 95/0/5	15 94/0/6	10 94/0/6
ISSCh 80	12 75/11/14	9 80/6/14	8 80/6/14	8 78/8/14	8 78/8/14
ISSCh 50	30 45/30/25	16 50/25/25	20 50/25/25	27 45/30/25	14 45/30/25
ISSCh 35	14 35/45/20	3 35/45/20	2 35/45/20	6 35/45/20	3 35/45/20
ISSCh 5	2 0/80/20	<1 0/80/20	<1 0/80/20	<1 0/80/20	<1 0/80/20
Kaolinite	5	4	7	8	8
KI R1	4	2	2	5	5
Chlorite	3	2	3	3	4
ICh 6		1 5/5/90	1 5/5/90		
Smectite					

Table S3b

Relative proportions (wt %) and compositions of the different mineral phases used to fit experimental XRD patterns of the 0.2-0.05 µm subfractions for 1904-2014 samples (CU and CF subplots). Values are given for composition in the Ca-EG state.

Contribution Ab. (%) / Comp.	1904 CU	1957 CU	1980 CU	1997 CU	2013 CU	2014 CU
Illite	7	1	2	1	1	1
ISSCh 90	10 94/2/4	7 95/1/4	9 95/1/4	8 95/1/4	11 93/2/5	16 93/2/5
ISSCh 80	9 80/6/14	13 76/10/14	10 76/10/14	11 73/13/14	16 75/11/14	13 75/11/14
ISSCh 50	44 56/19/25	40 58/17/25	35 58/17/25	39 56/19/25	39 50/25/25	35 50/25/25
ISSCh 35	16 35/45/20	23 38/42/20	21 38/42/20	22 36/44/20	15 30/50/20	13 30/50/20
ISSCh 5	2 10/70/20	3 10/70/20	3 5/75/20	2 0/80/20	1 0/80/0/20	1 0/80/20
Kaolinite	5	6	7	6	12	14
KI R1	6	6	10	9	4	6
Chlorite						
ICh 6	1 6/94	1 6/94	3 3/97	2 3/97	1 6/94	1 6/94
Smectite						
		1957 CF	**1980 CF**	**1997 CF**	**2013 CF**	**2014 CF**
Illite		8	2	1	1	1
ISSCh 90		9 95/1/4	8 95/1/4	8 95/1/4	15 93/2/5	16 92/4/4
ISSCh 80		8 76/10/14	12 76/10/14	16 73/13/14	13 75/11/14	17 78/8/14
ISSCh 50		43 50/25/25	42 50/25/25	41 58/17/25	35 54/20/25	35 52/24/24
ISSCh 35		16 35/45/20	17 30/50/20	14 38/42/20	14 30/50/20	14 30/50/20
ISSCh 5		3 5/75/20	1 5/75/20	1 0/80/20	1 0/80/20	1 0/80/20
Kaolinite		6	6	6	15	6
KI R1		5	10	11	5	9
Chlorite						
ICh 6		2 6/94	2 6/94	2 3/97	1 6/94	1 6/94
Smectite						

Table S3c

Relative proportions (wt %) and compositions of the different mineral phases used to fit experimental XRD patterns of the <0.05 µm subfractions for 1904-2014 samples (CU and CF subplots). Values are given for composition in the Ca-EG state.

Contribution Ab. (%) / Comp.	**1904 CU**	**1957 CU**	**1980 CU**	**1997 CU**	**2013 CU**	**2014 CU**
Illite						
ISSCh 90	15 88/8/4	7 89/6/4	9 90/7/4	8 90/6/4	10 90/6/4	9 89/7/4
ISSCh 80						
ISSCh 50	38 55/23/22	35 55/23/22	37 50/28/22	41 50/28/22	40 52/26/22	41 53/25/22
ISSCh 35	33 37/38/26	43 30/44/26	39 35/40/26	37 30/44/26	39 30/44/26	41 33/41/26
ISSCh 5	6 10/78/12	8 0/88/12	7 0/88/12	7 0/88/12	5 0/88/12	4 0/88/12
Kaolinite				0.4	1	
KI R1	7	5	6	5	4	4
Chlorite						
ICh 6						
Smectite	1	2	2	2	1	1
		1957 CF	**1980 CF**	**1997 CF**	**2013 CF**	**2014 CF**
Illite						
ISSCh 90		13 89/7/4	9 89/7/4	9 90/6/4	10 89/7/4	9 90/6/4
ISSCh 80						
ISSCh 50		38 52/26/22	43 50/28/22	36 50/28/22	38 50/28/22	32 52/26/22
ISSCh 35		36 30/44/26	31 30/44/26	40 30/44/26	41 30/44/26	44 35/44/26
ISSCh 5		6 0/88/12	9 0/88/12	9 0/88/12	5 0/88/12	9 0/88/12
Kaolinite						
KI R1		5	6	4	4	4
Chlorite						
ICh 6						
Smectite		2	2	2	2	2